October 2023

Stable Isotope Analysis on Yellowfin and Blackfin Tuna Eye Lenses Reveals Life History Patterns in the Gulf of Mexico

Kylee M. Rullo
University of South Florida

Stable Isotope Analysis on Yellowfin and Blackfin Tuna Eye Lenses Reveals Life History Patterns in the Gulf of Mexico

by

Kylee M. Rullo

A thesis submitted in partial fulfillment
of the requirements for the degree of
Master of Science
College of Marine Science
University of South Florida

Major Professor: Steven A. Murawski, Ph.D.
Ernst B. Peebles, Ph.D.
Julie L. Vecchio, Ph.D.

Date of Approval:
October 02, 2023

Keywords: Isoscape, Spatial movement, Trophic position, Ontogeny

ACKNOWLEDGMENTS

This research was made possible through the financial support of USF College of Marine Science Endowed Fellowships: the Von Rosenstiel Fellowship, the Paul Getting Endowed Memorial Fellowship, and the Carl Riggs Fellowship. Special thanks to the Florida Institute of Oceanography, the crews of the R/V *Weatherbird II* and F/V *The Gulf Eagle*, and everyone who participated in the field sampling efforts.

This work would not have been possible without the guidance and support of my advisor, Dr. Steven Murawski, and my committee members, Dr. Ernst Peebles and Dr. Julie Vecchio. Dr. Murawski contributed so much to this project and to my professional development as a scientist. I would also like to thank Dr. Vecchio especially for her guidance in eye-lens peeling and analytical methods. Thank you to Ethan Goddard for his contribution of equipment knowledge and his ability to troubleshoot expensive technology. I would also like to thank Sherryl Gilbert for organizing sampling trips, being available to answer my questions, and for always giving me Twizzlers when I needed them the most. Finally, I would like to thank my family (Donna, Gary, and Zac) and all of my friends for their unwavering love and support through this process.

TABLE OF CONTENTS

LIST OF TABLES

LIST OF FIGURES

ABSTRACT

Spatial geography, ontogenetic movement, and trophic patterns of mobile species are key elements of effective marine resource management. A number of methods are currently available for tracking movements of pelagic migratory species, including the use of conventional and electronic tags. However, tagging campaigns can take years to provide useful data, can be expensive, and only capture a portion of a fish's lifetime. For this project, I used stable-isotopic ratios of nitrogen ($\delta^{15}N$) and carbon ($\delta^{13}C$) in metabolically inert, chronologically-layered fish-eye lenses to explore lifetime movement and trophic patterns of yellowfin tuna (*Thunnus albacares*) and blackfin tuna (*Thunnus atlanticus*) in the Gulf of Mexico (GoM). In both species, the $\delta^{13}C$ values had a weak relationship with eye-lens diameter, reflecting a change in basal resource from cross-shelf movement. The $\delta^{15}N$ values were strongly correlated with eye-lens diameter, suggesting trophic growth and movement from areas with low $\delta^{15}N$ values to areas with high $\delta^{15}N$ values. Correlation between $\delta^{15}N$ and $\delta^{13}C$ was weak overall for both species, but some individual profiles displayed moderate to strong correlations that indicate alternate periods of migration and residency. Additionally, $\delta^{13}C$ values in the innermost laminae of yellowfin tuna were generally lower than the values in blackfin tuna, suggesting that spawning areas for these two species may be distinct. Despite the movement displayed in the profiles, the isotopic values were consistent with ranges previously measured in the GoM, so neither species appeared to exit the GoM. These results demonstrate that stable-isotopic ratios in eye lenses can be used successfully on pelagic fishes to determine broad life-history patterns.

CHAPTER ONE: STABLE ISOTOPE ANALYSIS ON YELLOWFIN AND BLACKFIN TUNA EYE LENSES REVEALS LIFE HISTORY PATTERNS IN THE GULF OF MEXICO

Introduction

The Gulf of Mexico

The Gulf of Mexico (GoM) is home to many ecologically, commercially, and recreationally important species (Chen 2017). In 2020, the United States' GoM commercial fisheries caught over 630,000 metric tons of seafood, which was valued at over $800 million and accounted for 15% of the United States' total commercial fishery catch and value (NMFS 2022). Fisheries in the GoM are managed in the United States on a regional level by the Gulf of Mexico Fishery Management Council which recommends fishery management plans to the National Marine Fisheries Service (NMFS). The GoM is also bordered by Mexico and Cuba, which each manage their own federal waters. Since the GoM is an interconnected ecosystem, management by three separate entities can make it difficult to regulate highly migratory species such as tunas, billfishes, and pelagic sharks. Regional fishery management organizations (RFMOs), such as the International Commission for the Conservation of Atlantic Tuna (ICCAT) to which all three GoM bordering countries belong, can coordinate international studies and apply appropriate regulation.

Since the GoM is a semi-enclosed sea bordered by three countries, it is greatly impacted by humans and human activity. One of the foremost human impacts on the GoM is oil and gas production and exploration. Thousands of oil and gas structures, both active and inactive, are located in the GoM off the coasts of the United States and Mexico, leading to unavoidable interactions between the platforms, the pollutants they produce, and marine life (Murawski et al. 2020). Other negative human impacts in the GoM include nutrient introduction, overfishing, and climate change (Karnauskas et al. 2017). Understanding the spatial geography and movements of GoM marine species can aid in conservation of important ecosystems and response measures for disasters like oil spills, particularly as migratory species cross international boundaries.

Yellowfin and Blackfin Tuna

Yellowfin tuna (YFT, *Thunnus albacares*) and blackfin tuna (BLFT, *Thunnus atlanticus*) are two highly migratory, pelagic species in the GoM. In 2020, the combined commercial and recreational reported landings of YFT in the U.S. GoM were around 300 metric tons and had an ex-vessel commercial value exceeding $1.6 million (NOAA Fisheries Office of Science and Technology 2020). BLFT, while not targeted by commercial fisheries in the U.S., are highly sought after by recreational anglers and are one of the most abundant tunas in the GoM (Cornic & Rooker 2018). Despite their importance as a fishery, a limited number of studies have been completed regarding YFT and BLFT movements and spatial geography in the GoM (Edwards and Sulak 2006, Weng et al. 2009, Hoolihan et al. 2014, Fenton 2015 et al., Ortiz 2017, Price et al. 2022).

Tuna distribution and range is mainly dependent on temperature (Boyce et al. 2008, Reglero et al. 2014). YFT are found worldwide in pelagic, tropical and sub-tropical environments and have been caught all around the GoM. They are found most often in the upper

100 m of the water column, but have been reported to dive to nearly 1000 m (Hoolihan et al. 2014). YFT exhibit a diel pattern, remaining closer to the surface at night and diving during the day (Weng et al. 2009, Hoolihan et al. 2014). BLFT have a more constrained range than YFT and are only found in the western Atlantic from Massachusetts to Rio de Janeiro, Brazil, including in the GoM. Like YFT, BLFT have a diel pattern of depth, remaining shallower at night and diving to depths up to 200 m during the day (Fenton et al. 2015). Both YFT and BLFT are opportunistic, sight-based predators, feeding mainly on fish, cephalopods, and crustaceans (Graham et al. 2007, Headley et al. 2009, Rudershausen et al. 2010, Lovell 2021); although, few diet studies for these species have been conducted in the GoM.

The U.S. GoM YFT fishery is managed by NMFS Highly Migratory Species Division, which implements the requirements of ICCAT. The BLFT fishery is not federally managed, but is included with other small tunas in ICCAT stock assessment reports. The ICCAT periodic stock assessments rely mainly on fishery-dependent data, using catch and effort across the Atlantic to estimate biomass and mortality (ICCAT 2019). While fishery-dependent data are important and useful in stock assessments, these data can often mischaracterize biological elements of the stock due to regulations (e.g., seasonal fishing closures) or gear limitations (Orbesen et al. 2017).

The common method to delimit stocks for management is to track spatial geography using tagging experiments. Tag returns can provide the basis of our understanding of fish movement, but tagging campaigns, particularly electronic tagging, can be quite expensive and require significant time to interpret life cycle patterns. Additionally, conventional tags only give the start and end location of the fish, and electronic tags are only programmed for a brief period of the fish's life and require interpolation of movement patterns between tagging sites and where

the popped-off transmitter is located. Conventional and electronic tagging campaigns have supplemented ICCAT stock assessments and given a basic understanding of YFT movement patterns (Ortiz 2017). The ICCAT conventional tagging campaign indicates that some YFT tagged in the GoM can travel across the Atlantic towards the Gulf of Guinea, but most are recaptured within the GoM (Ortiz 2017). Similarly, other electronic tagging studies have suggested long-term residencies of YFT, particularly around oil and gas platforms in the northern GoM (Edwards & Sulak 2006, Weng et al. 2009, Hoolihan et al. 2014). There are few movement studies of BLFT in the GoM, but a limited-duration, pop-up satellite archival tagging study conducted by Fenton et al. (2015) suggests that BLFT may display site fidelity particularly around oil and gas platforms.

Stable Isotope Analysis

An alternative method for determining fish movements, as well as trophic growth (i.e., the change in trophic position as the fish grows), is to employ stable isotopic ratios of nitrogen and carbon. The common forms of nitrogen (N) and carbon (C) are ^{14}N and ^{12}C, but each of these elements also exists in a heavier state (^{15}N and ^{13}C) in which the nucleus has an extra neutron (Fry 2006). The lighter and heavier states, known as isotopes, undergo similar chemical and biological processes but often at different rates and concentrations, which changes the ratio of the heavier to lighter isotope (Fry 2006). The change in ratio creates predictable trends in nature which can be measured using delta notation:

$$\delta X = \left(\frac{R_{sample}}{R_{standard}} - 1\right) \times 1000$$

where X is an element (C or N) and R is the isotope ratio of that element ($^{13}C/^{12}C$ or $^{15}N/^{14}N$). These predictable trends include trophic position increase and geographic trends.

Bulk values of $\delta^{15}N$ are enriched on average by 3.4‰ per trophic level which allows the relative trophic position to be estimated based on the $\delta^{15}N$ values of the primary producers of the ecosystem in which the fish lives (Post 2002, Fry 2006). Typically, as a fish grows, it consumes higher trophic position prey which in turn increases the $\delta^{15}N$ values within its tissues. Observed $\delta^{15}N$ values can also vary spatially. Nutrient introduction (e.g., river output or land runoff containing sewage or manure) can increase baseline $\delta^{15}N$ values (Hansson et al. 1997; Figure 1). Alternatively, nitrogen fixation, which occurs in oligotrophic waters, results in lower $\delta^{15}N$ values (Montoya et al. 2002, Fry 2006, Radabaugh et al. 2013; Figure 1).

Similar to $\delta^{15}N$ values, $\delta^{13}C$ is enriched with increasing trophic position; however, $\delta^{13}C$ only increases by 1‰ per trophic level on average which makes it more useful as a proxy for basal resource dependence (e.g., phytoplankton or benthic algae) and geographic location estimation (Fry 2006, Radabaugh et al. 2013, Vecchio et al. 2021). The $\delta^{13}C$ value generally decreases with ocean depth and is largely influenced by species composition of primary producers and primary production rates (Radabaugh et al. 2013). Higher $\delta^{13}C$ values are associated with increased growth rates of nearshore primary producers; additionally, nearshore benthic producers such as seagrasses and microalgae have higher $\delta^{13}C$ values than phytoplankton (Graham et al. 2010, Radabaugh et al. 2013; Figure 1).

Sampling stable isotopic values in tissues from primary producers, herbivores, omnivores, or predators allows researchers to create maps of isotopic spatial gradients, which are referred to as isoscapes (Graham et al. 2010, Peebles & Hollander 2020, Le-Alvarado et al. 2021). More sampling is required to create a high resolution isoscape in the GoM (particularly in offshore pelagic waters where tunas are abundant). However, the available isoscapes show a distinct gradient of stable isotopic values that make the GoM a viable location for determining

pelagic fish movements (Radabaugh et al. 2013, Le-Alvarado et al. 2021; Figure 1). To estimate fish movement, $\delta^{15}N$ and $\delta^{13}C$ values can be obtained from animal tissue and compared to an isoscape to determine the approximate position of the animal (Hobson et al. 2010).

Different tissues can be used for stable isotope analysis (SIA) of C and N including liver, muscle, and eye-lens tissues. Selecting the type of tissue used in SIA is primarily based on the turnover rate of tissues (time it takes for tissues to equilibrate to the isotopic profiles of their surroundings/prey items) are most relevant to the time scale of the study question. For example, while isotopic turnover rate can be variable within species, studies have consistently shown that stable isotopes in liver tissue turn over more quickly than those in muscle tissue (Logan et al. 2006, Madigan et al. 2012). In marine organisms, muscle typically turns over on the scale of months, so bulk stable isotope values within the muscle will be an average representation of several months prior to capture (Peebles & Hollander 2020).

In contrast, eye lenses contain lifetime stable isotope records. Fish eye lenses grow sequentially outwards in layers (laminae; Wistow & Piatigorsky 1988, Greiling & Clark 2012; Figure 2). Once a new lamina is added, the older lens layer undergoes attenuated apoptosis (cell death) to maintain eye-lens clarity with growth (Wride 2011). New protein synthesis cannot occur in older laminae after apoptosis, but the already-formed protein structures (crystallins) remain, preserving the isotopic record from the fish's diet at the time of the lens-layer formation (Wistow & Piatigorsky 1988, Tzadik et al. 2017). Analyzing each lamina individually allows for the creation of a chronological stable-isotope profile that spans from the first months of growth (the core of the eye lens) to the time of capture (the outer-most laminae).

Profiles of eye-lens stable isotope values versus eye-lens diameter give insight into a fish's life history. Vecchio et al. (2021) contrasted two demersal mesopredators (tilefish

Lopholatilus chamaeleonticeps and red grouper *Epinephelus morio*) to show how different life histories and movements are evident in $\delta^{15}N$ and $\delta^{13}C$ profiles. For the sedentary tilefish, there was a close correlation between $\delta^{15}N$ and $\delta^{13}C$ values, while the relationship for red grouper was more variable, reflecting movement across the isoscape. Eye-lens isotope profiles have also been explored for other teleosts (Wallace et al. 2014, 2023, Quaeck-Davies et al. 2018, Kurth et al. 2019, Curtis et al. 2020), squid (Meath et al. 2019), and elasmobranchs (Quaeck-Davies et al. 2018, Simpson et al. 2019). No eye-lens stable isotope studies have been completed on YFT or BLFT. Le-Alvarado et al. (2021) published a stable isotope study using YFT muscle and liver tissues. Their study suggested that the main feeding ground of YFT was the northern GoM, which compliments the tagging studies mentioned above (Edwards & Sulak 2006, Weng et al. 2009, Hoolihan et al. 2014). Le-Alvarado et al. (2021) also inferred that the YFT foraged in the central and southern GoM during spawning months, which could indicate that the southern GoM is an important, but underreported, spawning region for YFT. Additionally, Lovell (2021) compared northern GOM YFT diets to bulk $\delta^{15}N$ and $\delta^{34}S$ values (both of which can aid in determining diet changes) in muscle tissue and reported that both isotopic values and visual diet proportions fluctuated seasonally. Lovell (2021) also measured and compared $\delta^{13}C$ values in sub-adult and adult YFT tissue. They found $\delta^{13}C$ values were stable in adults, but had slight variation in sub-adults; Lovell (2021) suggests that the stability in adults could indicate residency in the northern GoM, while the variation in sub-adults could be due to trans-Atlantic individuals joining the GoM sub-adult class.

Objectives and Hypotheses

The goal of this study was to assess the use of eye-lens SIA as an indicator of both trophic growth and movement within the GoM isoscape in two pelagic, migratory species.

Specifically, I will (1) infer basal resource dependence and offshore/onshore movement from $\delta^{13}C$ profiles, (2) interpret the general trophic changes and north/south movement of YFT and BLFT using $\delta^{15}N$ profiles, and (3) use the $\delta^{15}N$ and $\delta^{13}C$ profiles together to interpret overall spatial movement and residency of the two species. The results of this research can be used to further the knowledge of habitat use of two economically important species, which can improve the understanding of stock boundaries and the effectiveness of fisheries management for the species. The null hypotheses that pertain to each objective are as follows:

1. There is no significant relationship or correlation between $\delta^{13}C$ and laminar midpoint (LM) within species or within individuals.
2. There is no significant relationship or correlation between $\delta^{15}N$ and LM within species or within individuals.
3. There is no significant relationship or correlation between $\delta^{13}C$ and $\delta^{15}N$ over time within species or within individuals.

Methods

Field Collections

A total of 46 YFT and 31 BLFT were used in this study and were collected by the Murawski lab at the University of South Florida during three sampling trips (Table 1). The majority of fish were collected in February 2020 from a rod and reel charter trip off the Texas coast that targeted tuna around oil platforms; the other 7 YFT were caught in the north-central GoM in 2018 and 2 BLFT were caught in the north-central GoM in 2022 (Table 1; Figure 3). After capture, individuals were measured at least to the precision of curved cm fork length (CFL, FL for the purpose of this study). Whole eyes were removed by severing the surrounding tissues

and the optic nerve, taking care to not puncture the globe of the eye. The globe was then wrapped in aluminum foil, placed in a plastic bag, and immediately frozen at -20°C.

Laboratory Processing

Eye lenses were delaminated and processed following Wallace et al. (2014, 2023) and Vecchio et al. (2021). Each lens was removed from the thawed eye by making an incision in the cornea, extracting the lens with forceps, and removing the lens capsule. The lens was then partially submerged in deionized water under a dissecting microscope. Laminae were separated into the thinnest layers mechanically possible by using fine-tipped forceps to start peeling at one lens pole and following the striation to the other lens pole (Figure 2). The peeling process was repeated around the lens until the lens surface appeared uniform. Before the start of delamination and between each laminar removal, the eye lens diameter (ELD) was measured at the widest point of the lens with a digital caliper to the nearest 0.01 mm (Figure 2). The laminar midpoint (LM) was then calculated as the average between the ELD before removal and the ELD after removal (Figure 2). The lens was considered fully delaminated once the laminae could no longer be mechanically separated; this was considered the core of the lens. Laminae were placed in individual microcentrifuge tubes and dried in an oven at 45°C for 12 hours.

After desiccation, the laminae were prepared for Elemental Analyzer Continuous Flow Isotope Ratio Mass Spectrometry (EA-IRMS). Individual lamina samples between 0.150 and 0.600 mg were weighed into 3.3 x 5 mm tin capsules using a Mettler Toledo® microbalance. The capsules were then folded and placed into the sample tray. Two samples were taken from each lamina so that the layers could be analyzed in duplicate for statistical reproducibility; if a core or other lamina was too small to duplicate, it was run as a single sample.

Nitrogen and carbon isotope and bulk composition were measured using a Carlo-Erba® EA1108 Elemental Analyzer coupled with a ThermoFinnagan® Delta + XL IRMS in the Marine Environmental Chemistry Laboratory at the University of South Florida College of Marine Science in St. Petersburg, FL. The standard reference materials used for isotope scale and elemental calibration were NIST 8573 and NIST 8574 L-glutamic acid. The laboratory reference used for quality control was NIST 1577b (bovine liver) with an analytical uncertainty of ±0.10‰ for $\delta^{13}C$ and ±0.17‰ for $\delta^{15}N$. Results are reported in per mil (‰) notation and scaled to Vienna Pee Dee Belemnite for $\delta^{13}C$ and the accepted standard of air for $\delta^{15}N$:

$$\delta X = \left(\frac{R_{sample}}{R_{standard}} - 1\right) \times 1000$$

where X is an element (C or N) and R is the isotope ratio of that element ($^{13}C/^{12}C$ or $^{15}N/^{14}N$).

Data Analysis

All statistical analyses were completed in R statistical software version 4.2.2 (R-Core-Team 2022). The overall mean, standard error, minimum, maximum and range $\delta^{13}C$ and $\delta^{15}N$ values were calculated for each YFT and BLFT. A PERMDISPER routine was used to test for multivariate dispersion in isotopic ratios between YFT and BLFT, and a subsequent PERMANOVA statistically tested for differences in $\delta^{13}C$ and $\delta^{15}N$ values between the two species (package 'vegan,' Oksanen et al. 2019).

Since eye lenses do not display age marks, a best-fit regression through the origin was constructed to describe the relationship between the maximum ELD and FL at time of capture for each species. One YFT and three BLFT were not included in the linear regression as they did not have a recorded FL, likely due to predation on body parts. For YFT, the linear equation used was FL (cm) = 7.98 × ELD (mm) ($F = 5147$, $R^2 = 0.99$, $p < 0.001$; Figure 4). For BLFT, the

linear equation used was FL (cm) = 5.36 × ELD (mm) (F = 4964, R^2 = 0.99, p < 0.001; Figure 4). Estimated age of the fish could then be extrapolated from the calculated FL using a fitted Richard's growth curve:

$$L_t = L_\infty[1 - ae^{(-kt)}]^b$$

where L_t is length at age t, L_∞ is the average maximum length (YFT = 1658 mm, BLFT = 907 mm), a is the parameter that controls the horizontal inflection point (YFT = 1.04, BLFT = 1.05), k is the growth rate (YFT = 0.23 y^{-1}, BLFT = 0.112 y^{-1}), and b is the parameter that controls the vertical inflection point (YFT = 0.45, BLFT = 0.25; Paccico et al. 2021, Gutierrez 2022). A LOESS curve was also fitted to each species during each capture year to observe any strong patterns in isotopic value.

The mean, standard error, minimum, maximum, and range $\delta^{13}C$ and $\delta^{15}N$ values were evaluated for the cores, outer laminae, and lifetime changes of each species. Lifetime change was calculated as an individual's innermost laminar isotopic value subtracted from its outermost laminar isotopic value, and was used to quantify the net increase or decrease in $\delta^{13}C$ or $\delta^{15}N$ values during an individual's life.

The relationships between isotopic values and LM were modeled by a logarithmic curve in the form of $\delta X = a + b \times \ln(LM)$, where δX is $\delta^{13}C$ or $\delta^{15}N$, a is the parameter controlling the vertical shift of the curve, and b is the parameter controlling the shape of the curve. This model is representative of growth equations commonly used for fish (von Bertalanffy 1938, Ricker 1975) and assumes trophic position mirrors fish growth. The modeled trends in isotopic values can be attributed to changes in trophic position with growth of the fish. Deviations from the modeled curves can indicate movement across the isotopic gradient or a change in basal resource (Vecchio et al. 2021). To further interpret the deviations from the logarithmic curve, mean

absolute deviation (MAD) was calculated for each species and each individual using the model-predicted isotopic values and the measured isotopic values:

$$MAD = \frac{\sum_{i=1}^{n} \left| \delta X_{measured} - \delta X_{predicted} \right|}{n}$$

where δX is $\delta^{13}C$ or $\delta^{15}N$ and n is the number of laminae for each fish. A larger relative MAD indicated a fish that likely moved across isotopic gradients or changed basal resources throughout its lifetime.

To determine the relationship between $\delta^{13}C$ and $\delta^{15}N$ for each species, a linear mixed effect model using individual fish as random effect was constructed with the R package 'lme4' (Bates et al. 2015). A significant, positive relationship between $\delta^{13}C$ and $\delta^{15}N$ would indicate that the individuals within a species increased in trophic position throughout their lifetimes and did not experience movement across an isotopic gradient or change basal resources.

Correlations were used to further aid in separating trophic growth from spatial movement. Spearman rank correlations (r_s) were employed to assess the independence of two variables and test for a monotonic relationship between those variables. The series of three correlations were as follows:

1). Correlation between $\delta^{13}C$ and LM in individual (or species) eye lenses: Has the fish shown movement along the $\delta^{13}C$ gradient or changed basal resources during its lifetime?

2). Correlation between $\delta^{15}N$ and LM in individual (or species) eye lenses: Has the fish shown trophic growth or movement along the $\delta^{15}N$ gradient during its lifetime?

3). Correlation between $\delta^{15}N$ and $\delta^{13}C$ in individual (or species) eye lenses: Is there consistency between the two isotopes throughout a fish's lifetime?

Correlations were evaluated based on conventional terminology: 0-0.19 = very weak, 0.20-0.39 = weak, 0.40-0.59 = moderate, 0.60-0.79 = strong, and 0.80-1 = very strong. Interpretations of

these correlations follow Vecchio et al. (2021) "isotopic outcomes" (Figure 5). Strong correlations indicated that the fish likely increased in trophic position with no movement across the isotopic gradient during its lifetime. Weak correlations required further interpretation using the isotopic outcomes to understand the lack of relationship between the variables.

Results

Biometric and Isotopic Species' Overviews

A total of 814 YFT laminae and 495 BLFT laminae were studied using SIA. Individual YFT ranged from 80 to 166 cm FL, with maximum ELD ranging from 9.86 to 20.11 mm (Table 2). Based on the FL at time of capture and the fitted Richard's growth curve, 33 YFT were between ages one and two, 5 YFT were between ages two and three, and 8 YFT were greater than age three (Paccico et al. 2021). Individual BLFT ranged from 48 to 88 cm FL, with maximum ELD ranging from 8.38 mm to 16.80 mm (Table 3). Based on the estimated FL and the fitted Richard's growth curve, 9 BLFT were between ages one and two, 15 BLFT were between ages two and three, and 7 BLFT were greater than age three (Gutierrez 2022).

Mean (± SE) $\delta^{13}C$ value for all YFT laminae was -17.89‰ ± 0.02, ranging from -19.73‰ to -16.18‰, and mean (± SE) $\delta^{15}N$ value was 8.19‰ ± 0.05, ranging from 3.54‰ to 13.57‰ (Figure 6). When compared to YFT as a whole, BLFT had a broader range of values for both $\delta^{13}C$ and $\delta^{15}N$, had a higher mean $\delta^{13}C$ value, and had a lower mean $\delta^{15}N$ value. Mean (± SE) $\delta^{13}C$ value for all BLFT laminae was -17.75‰ ± 0.02, ranging from -19.85‰ to -16.12‰, and mean (± SE) $\delta^{15}N$ value was 7.98‰ ± 0.08, ranging from 3.61‰ to 14.47‰ (Figure 6).

Both the PERMANOVA and PERMDISPER result examining the difference in stable isotope values between the two species were significant (PERMANOVA: $F = 6.7$, $p < 0.01$; PERMDISPER: $F = 11.62$, $p < 0.01$. Since the homogenous dispersion assumption of

PERMANOVA was not met, the significant PERMANOVA result cannot be definitively interpreted as a difference in isotopic values between YFT and BLFT. However, the significant PERMDISPER indicates that there is a difference in multivariate dispersion between the two species.

Lifetime Isotopic Profiles

Core diameters for YFT measured between 0.47 mm (estimated FL = 3.75 cm) and 2.77 mm (estimated FL = 22.11 cm). Six YFT cores were lost during analysis, so the individuals were excluded from mean core isotopic value calculations. YFT cores had a mean (± SE) $\delta^{13}C$ value of -18.76 ± 0.08‰, and YFT outer laminae had a mean (± SE) $\delta^{13}C$ value of -17.49 ± 0.08‰ (Figure 7). The isotopic profiles were examined for lifetime change in isotope value by subtracting the core (representing the youngest fish age) from the outermost lamina (representing age of capture) in each individual. In cases where the core was lost, the fish were excluded from lifetime change analyses. All YFT, except for the individual with the smallest ELD, increased in $\delta^{13}C$ value from their core to their outermost laminae. Mean (± SE) $\delta^{13}C$ lifetime change for YFT was 1.27 ± 0.11‰, ranging from -0.58‰ to 2.60‰ (Table 2).

Visual inspection of the individual lifetime profiles indicates a general $\delta^{13}C$ spike in the earlier stages of life, followed by a sharp decrease and subsequent increase in $\delta^{13}C$ for many of the YFT (Figure 8). This is further supported by the LOESS curve for YFT which shows an initial increase in $\delta^{13}C$, followed by a $\delta^{13}C$ dip around age one (Figure 9). YFT from both years had a similar increase in $\delta^{13}C$ at the beginning, but the 2018 fish appear to have subsequently higher $\delta^{13}C$ values than the 2020 individuals (Figure 9).

YFT cores had a mean (± SE) $\delta^{15}N$ value of 5.87 ± 0.22‰, and YFT outer laminae had a mean (± SE) $\delta^{15}N$ value of 10.29 ± 0.14‰ (Figure 7). All individual YFT had positive lifetime

changes in $\delta^{15}N$. Excluding YFT with lost cores, the mean (± SE) $\delta^{15}N$ lifetime change was 4.47 ± 0.27‰, ranging from 0.96‰ to 8.38‰ (Table 2). Closer inspection of the profiles revealed the lowest $\delta^{15}N$ value for each YFT occurred before a LM of 5.2 mm (estimated FL = 41.50 cm) in all of the fish, but the lifetime patterns in $\delta^{15}N$ profiles varied by individual (Figure 10). The LOESS curves for YFT $\delta^{15}N$ shows an increase in $\delta^{15}N$ with hardly any variation in the curve (Figure 9). The 2018 and 2020 curves mirror each other closely (Figure 9).

The core diameters for BLFT were between 0.54 mm (estimated Fl = 2.89 cm) and 3.19 mm (estimated FL = 17.10 cm). Four BLFT cores were lost during analysis, so the individuals were excluded from mean core isotopic value calculations. BLFT cores had a mean (± SE) $\delta^{13}C$ value of -18.00 ± 0.09‰, and BLFT outer laminae had a mean (± SE) $\delta^{13}C$ value of 17.51‰ ± 0.07 (Figure 7). Of the 27 BLFT included in lifetime change analysis, 25 individuals increased in $\delta^{13}C$ from their core to their outermost laminae. Mean (± SE) $\delta^{13}C$ lifetime change for BLFT was 0.52‰ ± 0.11, ranging from -1.61‰ to 1.81‰ (Table 3).

Visual inspection shows variation in the $\delta^{13}C$ among BLFT individuals, although most appear to have a pattern similar to YFT with a $\delta^{13}C$ during the first year of life, followed by a decrease in $\delta^{13}C$ between a LM of 5 mm and 10 mm, and a subsequent increase before time of capture (Figure 11). This is further supported by the LOESS curve for BLFT which shows an initial increase in $\delta^{13}C$, followed by a $\delta^{13}C$ dip around age one (Figure 12). BLFT from both years have a similar pattern in $\delta^{13}C$, but the 2022 fish appear to have consistently higher $\delta^{13}C$ values than the 2020 individuals (Figure 12). However, it should be noted that the 2022 LOESS curve is only based on two individuals.

BLFT cores had a mean (± SE) $\delta^{15}N$ value of 5.14‰ ± 0.19, and BLFT outer laminae had a mean (± SE) $\delta^{15}N$ value of 10.19‰ ± 0.20 (Figure 7). All individual BLFT had positive

lifetime changes in $\delta^{15}N$. Excluding BLFT with lost cores, the mean (± SE) $\delta^{15}N$ lifetime change was 5.06‰ ± 0.29, ranging from 3.03‰ to 10.61‰ (Table 3). Closer inspection of the profiles revealed the lowest $\delta^{15}N$ value for each BLFT occurred before a LM of 2.7 mm in every fish, and all individuals shared similar increasing patterns in $\delta^{15}N$ across their lifetimes (Figure 11). The LOESS curves for BLFT $\delta^{15}N$ show a rapid increase in $\delta^{15}N$ before age one, followed by a slower rate of increase after age one (Figure 12). Like with the $\delta^{13}C$ curves, the 2022 BLFT appear to have consistently higher $\delta^{15}N$ values than the 2020 BLFT (Figure 12).

Modeling the Relationships between $\delta^{13}C$, $\delta^{15}N$, and LM

In YFT, the positive logarithmic relationship between $\delta^{13}C$ and LM was significant, but the variability was not well-explained by the model fit (R^2 = 0.19, F = 195.9, p < 0.001; Figure 14). The overall MAD for YFT $\delta^{13}C$ values was 0.42‰ (Table 2). The majority of YFT individuals varied less than 0.60‰ on average from the modeled $\delta^{13}C$ values, with individual MAD values ranging from 0.16‰ to 0.94‰ (Table 2; Figure 8). The positive logarithmic relationship between $\delta^{15}N$ and LM in YFT was significant, and the variability was moderately explained by the model fit (R^2 = 0.49, F = 767.8, p <0.001; Figure 14). The overall MAD for YFT $\delta^{15}N$ values was 0.82‰ (Table 2). MAD for individual YFT $\delta^{15}N$ values ranged from 0.32‰ to 1.85‰ (Table 2; Figure 10). The linear mixed effect model for $\delta^{15}N$ and $\delta^{13}C$ values did not converge in YFT (Figure 14).

In BLFT, the positive logarithmic relationship between $\delta^{13}C$ and LM was very weak and variability was not well-explained by the model fit (R^2 = 0.01, F = 5.86, p = 0.02; Figure 13). The overall MAD for BLFT $\delta^{13}C$ values was 0.36‰ (Table 3). MAD for individual BLFT $\delta^{13}C$ values ranged from 0.16‰ to 0.63‰ (Table 3; Figure 11). The positive logarithmic relationship between $\delta^{15}N$ and LM in BLFT was significant and variability was well-explained by the model

fit (R^2 = 0.64, F = 866.8, p < 0.001; Figure 14). The overall MAD for BLFT $\delta^{15}N$ values was 0.85‰ (Table 3). The majority of $\delta^{15}N$ values for BLFT individuals varied less than 1.00‰ on average from the modeled $\delta^{15}N$ values, with MAD values ranging from 0.40‰ to 1.92‰ (Table 3; Figure 13). Like in YFT, the BLFT linear mixed effect model for $\delta^{15}N$ and $\delta^{13}C$ values did not converge (Figure 14).

Correlations

For all combined YFT laminae, the Spearman rank coefficient (ρ) between $\delta^{13}C$ values and LMs was weak but significant (ρ = 0.34, p < 0.001; Table 3). The $\delta^{13}C$ values were significantly correlated with LM in 22 YFT profiles; of those 22 individuals, 18 individuals had moderate to very strong positive correlations, and four had moderate to strong negative correlations (Table 2). The Spearman rank coefficient between $\delta^{15}N$ values and LMs in all YFT laminae was significant, positive, and strong (ρ = 0.75, p < 0.001; Table 2). The $\delta^{15}N$ values were significantly correlated with LMs in 42 YFT individuals, with the majority being very strong correlations (Table 2). The correlation between $\delta^{15}N$ and $\delta^{13}C$ values for all YFT laminae was very weak, but significant (ρ = 0.12, p < 0.001; Table 3). The relationship between isotopic values was significant in 21 YFT individuals, with moderate to very strong positive correlations in 15 fish, moderate to very strong negative correlations in five fish, and a weak positive correlation in one fish (Table 2, Figure 15).

For all combined BLFT laminae, the coefficient correlating $\delta^{13}C$ values and LMs was not significant (ρ = 0.02, p > 0.05; Table 3). The $\delta^{13}C$ values were significantly correlated with LMs in only seven BLFT profiles, with four individuals having moderate to strong positive correlations and three having strong negative correlations (Table 3). The Spearman rank coefficient correlating $\delta^{15}N$ values and LMs in all BLFT laminae was significant, positive, and

very strong ($\rho = 0.88$, $p < 0.001$; Table 3). The $\delta^{15}N$ values were significantly correlated with LMs in all 31 of the individual BLFT, with the majority being very strong correlations (Table 3). The correlation between $\delta^{15}N$ and $\delta^{13}C$ values for all BLFT was very weak and negative, but significant ($\rho = -0.15$, $p < 0.001$; Table 3). The relationship between isotopic values was significant in seven BLFT individuals, with strong and very strong positive correlations in two fish, and very strong negative correlations in five fish (Table 3, Figure 16).

Discussion

Stable isotope analysis of YFT and BLFT eye lenses supports the movement of these two species across the GoM isoscape, but indicates that individuals may have extended periods of residency in an area during their lifetime. When plotted against LM, the $\delta^{13}C$ profiles were used to interpret onshore or offshore movement of the fish and the $\delta^{15}N$ profiles were used to assess trophic changes and latitudinal movement throughout an individual's lifetime. Used together, the stable isotope profiles depict the overall movement for the fishes within the GoM. Nonlinear regressions, deviations from predicted values, lifetime isotopic changes, and Spearman rank coefficients of correlation were used to quantify and qualify the patterns observed in the profiles. As compared to the use of other tissues (e.g. muscle, liver), the use of eye-lens laminae do not require any consideration of turnover rate of the tissues in interpreting movement, and, with multiple laminae, the record of isoscape occupancy and trophic position is essentially continuous.

Onshore/Offshore Movement from $\delta^{13}C$ Profiles

Nearshore benthic basal resources typically have higher $\delta^{13}C$ values than offshore planktonic basal resources (Graham et al. 2010, Radabaugh et al. 2013); conversely, Le-

Alvarado et al. (2021) reports some of the lowest $\delta^{13}C$ values inshore on the Texas-Louisiana shelf, with $\delta^{13}C$ values increasing offshore. Since the scale and sampling techniques differ among isoscape studies, it is difficult to reconcile variations among overlapping isoscapes; however, the broad pattern in the GoM appears to be lower $\delta^{13}C$ values in the northwest compared to other areas, with small scale patterns indicating higher $\delta^{13}C$ values inshore and lower $\delta^{13}C$ values offshore. Using these trends, lifetime movement across the $\delta^{13}C$ isoscape can be inferred from the values measured in eye-lens laminae.

The core of an eye lens contains isotopic records from the earliest life-stages of a fish and can provide insights into the spawning grounds of YFT and BLFT (Vecchio and Peebles 2020). Cores from YFT had a lower mean $\delta^{13}C$ value than cores from BLFT, indicating that YFT spawn further offshore than BLFT. The LOESS models also support YFT initially remaining in lower $\delta^{13}C$ environments than BLFT, despite both species increasing in $\delta^{13}C$ during this time. The early increase in the $\delta^{13}C$ LOESS models is potentially due to switching basal resources as juvenile fish move further inshore from their respective spawning grounds. Around age one, $\delta^{13}C$ decreases, indicating another likely basal resource change as the fish move back offshore. The pattern displayed in the LOESS models is potentially seasonal or ontogenetic movement of these two species. Since tuna distribution is mainly dependent on temperature, YFT and BLFT may undergo small- or large-scale horizontal movements with seasonally-changing water temperatures that allow them to remain in their preferred temperature ranges (Boyce et al. 2008, Weng et al. 2009, Hoolihan et al. 2014). Additionally, as a tuna grows, its temperature range and prey item size will increase (Boyce et al. 2008, Cornic et al. 2017), which could explain the movement to a lower $\delta^{13}C$ environment around age one for both YFT and BLFT. This bump in

$\delta^{13}C$ eye-lens profiles has also been documented in red grouper, a species known to move inshore as juveniles and return offshore as they reach sexual maturity (Vecchio et al. 2021).

Both species had poor fits between the data and the logarithmic model between $\delta^{13}C$ and LM, as well as weak overall correlations between $\delta^{13}C$ and LM. The weak relationship between $\delta^{13}C$ and LM further supports the likelihood of cross-shelf movements by BLFT and YFT. As a species, BLFT had a weaker relationship between $\delta^{13}C$ and LM than YFT, appearing to switch basal resources more often than YFT. This idea of multiple cross-shelf movements by BLFT is supported in literature and anecdotally by recreational fishers since BLFT are often observed moving closer to shore than YFT, likely due to slightly differing temperature and prey preferences by the two species (Collette and Nauen 1983, Boyce et al. 2008, Weng et al.2009, Hoolihan et al. 2014, Fenton et al. 2015). Despite overall patterns of movement in YFT and BLFT, differing individual correlations and MAD values indicate that the scope of the movement across different $\delta^{13}C$ environments varied widely by individual.

Since all but one YFT and two BLFT had positive lifetime changes in $\delta^{13}C$, it is possible that some of the relationship between $\delta^{13}C$ and LM is due to trophic position increase. Organisms increase in $\delta^{13}C$ by approximately 1.0‰ per trophic position, although some variation in that number has been reported (McCutchan et al. 2003, Fry 2006, Matley et al. 2015). The mean lifetime change for YFT was 1.27‰ which equates to an average increase of 1 – 2 trophic positions if all of the increase was due to increasing trophic position. The mean lifetime change for BLFT was 0.55‰ which equates to an average increase of 0 – 1 trophic positions. Adult YFT and BLFT occupy high trophic positions, so a change of 1 – 2 trophic positions from larvae to sub-adult or adult would be expected (Olson & Watters 2003, Popp et al. 2007, Headley et al. 2009, Albuquerque et al. 2019, Le-Alvarado et al. 2021).

Movement and Trophic Interpretation from $\delta^{15}N$ profiles

All individuals from both species increased in $\delta^{15}N$ value from early life to time of capture, but not monotonically. This was reflected by the Spearman rank coefficients in which the majority of individuals displayed very strong correlations between $\delta^{15}N$ and LM. The YFT that did not have strong correlations moved inconsistently, likely migrating against the $\delta^{15}N$ gradient while increasing in trophic position. As a species, BLFT had a stronger nonlinear relationship in the data and a stronger overall correlation between $\delta^{15}N$ and LM than YFT, suggesting that YFT as a species moves more often across the $\delta^{15}N$ gradient than BLFT. Similar to $\delta^{13}C$, an increase in $\delta^{15}N$ with age is expected because of trophic position increase. However, separating spatial movement, or lack thereof, from trophic growth is difficult, and two different interpretations can be inferred from the significant nonlinear relationship and strong correlations based on known life history patterns of the species.

The first spatial interpretation is that most individuals moved with the $\delta^{15}N$ gradient, migrating from the southern/central GoM to the northern GoM. The nonlinear relationship between $\delta^{15}N$ and LM coupled with the individually-variable correlations between $\delta^{13}C$ and LM suggest at least some spatial movement during both species' lifetimes. Specifically, $\delta^{15}N$ values in YFT were only moderately represented by the logarithmic relationship, indicating that more than trophic growth was occurring. The southern/central GoM is not typically considered an important spawning ground for YFT or BLFT, but larvae of both species have been documented in the region (Espinosa-Fuentes et al. 2013, Reglero et al. 2014) and in the Florida Straits (Richardson et al. 2010), so it is possible that individuals with increasing $\delta^{15}N$ profiles migrated from the southern/central GoM to the northern GoM where $\delta^{15}N$ values are the highest (Radabaugh et al. 2013, Le-Alvarado et al. 2021). Le-Alvarado et al. (2021) also noted in a liver-

and muscle-based stable isotope study that YFT had likely fed in the southern/central GoM during spawning season.

The second interpretation for the strong correlations between $\delta^{15}N$ and LM is that the majority of individuals increased in trophic position throughout their lifetime without Gulf-wide movement. This interpretation seems more likely due to the core $\delta^{15}N$ values, the age and size of the individuals, and the scale of the lifetime change. For both species, the mean core $\delta^{15}N$ value was more consistent with $\delta^{15}N$ values measured from zooplankton samples in the northern GoM than the southern/central GoM (Le-Alvarado et al. 2021). The northern GoM is a known spawning habitat for both YFT and BLFT (Grimes & Finucane 1991, Lang et al. 1994, Arocha et al. 2001, Cornic & Rooker 2018) and may serve as an important larval and juvenile nursery (Lang et al. 1994, Cornic & Rooker 2018, 2021), so it would not be surprising for younger, smaller fish to remain in the northern GoM. Furthermore, the mean lifetime change of $\delta^{15}N$ values in YFT and BLFT was 4.28‰ and 4.98%, respectively. Like with $\delta^{13}C$ values, the values of $\delta^{15}N$ are expected to increase with increasing trophic position. The average increase in $\delta^{15}N$ value per trophic position is 3.4‰, but this number is variable depending on the content of the consumer's diet (McCutchan et al. 2003, Fry 2006, Matley et al. 2015). For both species, the average change in $\delta^{15}N$ values would equate to a 1 – 2 trophic position increase, similar to the trophic position change in $\delta^{13}C$ values. Again, since these species occupy high trophic positions, an increase of this magnitude is expected (Olson & Watters 2003, Popp et al. 2007, Headley et al. 2009, Albuquerque et al. 2019, Le-Alvarado et al. 2021).

Periods of Residency from $\delta^{15}N$ and $\delta^{13}C$ Correlations

The linear mixed effect model evaluating the relationship between $\delta^{15}N$ and $\delta^{13}C$ did not converge in either species, and the overall correlation for both species was weak. In a species

that makes no movements across isotopic gradients, the relationship between $\delta^{15}N$ and $\delta^{13}C$ would be positive and strong since both $\delta^{15}N$ and $\delta^{13}C$ would be increasing together as trophic position increased, with no variations due to changing basal resources (Vecchio et al. 2021). Therefore, the poor relationship between $\delta^{15}N$ and $\delta^{13}C$ in YFT and BLFT indicates lifetime movement across isotopic gradients. However, the strength of the correlation varied among individual profiles. A visual inspection of the 15 YFT and 2 BLFT profiles that had significant, positive correlations between $\delta^{15}N$ and $\delta^{13}C$ shows an inconsistent increase throughout the individuals' lives. These fish may have had both periods of residency and periods of movement within their lifetimes. For YFT, these results are consistent with the results of tagging studies that suggest some individuals may reside in one area for weeks, or even months, at a time (Klimley et al. 2003, Edwards & Sulak 2006, Hoolihan et al. 2014, Price et al. 2022). Fewer studies have been conducted on BLFT, but evidence exists that they too may have periods of residency in a single region (Fenton et al. 2015). The northern GoM has numerous deepwater oil platforms that may act as fish aggregating devices (FAD) for pelagic, migratory fishes (Edwards & Sulak 2006, Hoolihan et al. 2014, Snodgrass et al. 2020, Price et al. 2022). Since the majority of our study fish were caught around oil platforms, it is possible that the individuals with significant, positive correlations between $\delta^{15}N$ and $\delta^{13}C$ are aggregating around these platforms for extended periods, essentially becoming residents for those periods.

The few YFT and BLFT individuals that showed significant negative correlations between $\delta^{15}N$ and $\delta^{13}C$ likely moved with the $\delta^{15}N$ gradient and against the $\delta^{13}C$ gradient. This supports the interpretation that some individuals migrated from the southern/central GoM (lower $\delta^{15}N$, higher $\delta^{13}C$) to the northern GoM (higher $\delta^{15}N$, lower $\delta^{13}C$). The remaining individuals

that had weak or insignificant correlations between $\delta^{15}N$ and $\delta^{13}C$ likely moved inconsistently across isotope gradients throughout their lives.

Conclusions

In this study, I show that bulk SIA can be used successfully to reveal general life history patterns in pelagic, migratory species and addressed each of my three null hypotheses:

1. There was an overall significant, nonlinear relationship and significant correlation between $\delta^{13}C$ and LM for both species; however, the nonlinear relationships did not describe a majority of the variation in the data and the correlations were weak, suggesting that both species switch between planktonic and benthic basal resources. BLFT, in particular, had a weak relationship between $\delta^{13}C$ and LM, appearing to make multiple cross-shelf movements. Additionally, the strength of individual correlations between $\delta^{13}C$ and LM varied widely for both species, demonstrating that pelagic, migratory species do not necessarily display similar individual patterns of movement throughout their lifetimes. However, the LOESS smooths revealed a possible seasonal or ontogenetic pattern in which both species appeared to move from lower, offshore $\delta^{13}C$ environments to higher, inshore $\delta^{13}C$ environments before returning offshore before or around age 1. Though both species displayed this carbon bump, YFT appeared to originate and remain in lower $\delta^{13}C$ environments than BLFT, indicating that these species have separate spawning environments.
2. There was an overall significant, nonlinear relationship and significant correlation between $\delta^{15}N$ and LM for both species, and the majority of individuals had strong to very strong correlations. One explanation for this pattern is that the fish travelled from the southern/central GoM with lower $\delta^{15}N$ values to the northern GoM with higher $\delta^{15}N$.

While some individuals with varying $\delta^{15}N$ profiles may have undergone this northern migration, the average lifetime changes in $\delta^{15}N$ for both species equated to the expected trophic position increase. The mean $\delta^{15}N$ core values for both species were also more consistent with northern $\delta^{15}N$ GoM values. The second explanation is that the individuals were residents in the northern GoM (possibly around the oil platforms where they were captured) and the increase in $\delta^{15}N$ is mostly due to increasing trophic position. This explanation appears to be more likely for the majority of individuals based on overall species values and patterns.

3. The linear mixed effect model between $\delta^{15}N$ and $\delta^{13}C$ did not converge for either species, and the overall correlation was significant, but weak for both species. Since the $\delta^{15}N$ and $\delta^{13}C$ was decoupled, the fish likely did not remain in one location their entire lives. However, some individuals did display significant, strong correlations between $\delta^{15}N$ and $\delta^{13}C$, suggesting possible periods of residency. The few negative correlations in YFT may indicate that some fish traveled from the southern/central GoM (low $\delta^{15}N$, high $\delta^{13}C$) to the northern GoM (high $\delta^{15}N$, low $\delta^{13}C$).

Both YFT and BLFT are important fisheries species in the GoM, yet their migration and trophic patterns are not well-documented in the literature. To further separate migration patterns from trophic patterns, we can use compound-specific stable isotope analysis, which allows for calculations that isolate trophic growth from movement across an isotopic gradient (Harada et al. 2022, Wallace et al. 2023). Additional tagging and diet studies can also be helpful baselines when teasing apart movement and trophic growth, particularly in the GoM, and increasing the number of larval studies in the southern/central GoM may aid in determining new locations of tuna spawning grounds.

This study was restricted to only YFT and BLFT collected in the northern GoM and limited by inconsistent GoM isoscape measurements. Future research could include collecting tuna and other pelagic species in each region of the GoM and comparing their lifetime isotopic values to determine any common patterns that could indicate seasonal or ontogenetic changes. Designating a consistent sampling procedure for measuring the isoscape would also lessen the uncertainty when comparing isotopic values in fish tissues to the background environment.

Tables and Figures

Table 1: Collection and station information for all sample sites in the northern GoM. Average water depth rounded to the nearest 10 m.

Year	Month	Gear Used	Stations	Avg Water Depth (m)	YFT	BLFT
2018	August	Pelagic Longline	B287	2780	1	-
			B282	2530	2	-
			B081	2320	1	-
			B001	860	2	-
			B251	1570	1	-
2020	February	Rod and Reel	Nansen	1200	2	21
			Hoover	-	-	2
			Perdido	2740	37	6
2022	May	Demersal Longline	SL9-150	290	-	1
		Rod and Reel	Troll	60	-	1
				Totals	**46**	**31**

Table 2: Individual YFT information ordered by decreasing eye lens diameter (ELD). Number of eye lens laminae (ELL), fork length (FL), lifetime isotopic change (LC), mean absolute deviation from predicted isotopic values (MAD), and Spearman rank correlation coefficients (ρ) are listed. Means were calculated for ELD, ELL, FL, and LC, and MAD and correlation coefficients were calculated for all YFT combined.

Fish ID	ELD (mm)	ELL	FL (cm)	LC $\delta^{13}C$	LC $\delta^{15}N$	MAD $\delta^{13}C$	MAD $\delta^{15}N$	$\delta^{13}C$ vs LM ρ	$\delta^{15}N$ vs LM ρ	$\delta^{15}N$ vs $\delta^{13}C$ ρ
18-B251-D-002	20.11	25	166	2.51	7.06	0.44	1.05	0.62^{***}	0.94^{***}	0.62^{***}
18-B282-N-002	19.06	26	166	1.62	2.84	0.29	0.53	0.66^{***}	0.91^{***}	0.66^{***}
18-B001-D-001	17.25	24	156	2.60	6.86	0.36	0.96	0.25	0.97^{***}	0.36
18-B282-D-001	17.24	21	160	1.46	4.53	0.37	0.73	0.15	0.80^{***}	0.23
18-B287-D-003[+]	16.58	26				0.38	0.86	0.43^{*}	0.65^{***}	0.73^{***}
18-B081-D-003	16.56	28	140	2.10	5.70	0.38	1.31	0.98^{***}	0.54^{**}	0.54^{**}
18-B001-N-005	15.91	31	137	2.11	8.38	0.41	0.87	0.87^{***}	0.92^{***}	0.82^{***}
20-Nan-02	14.01	15	123	2.07	4.78	0.36	0.40	0.70^{**}	1.00^{***}	0.69^{**}
20-Per-22	13.53	16	117	1.24	5.59	0.47	0.37	−0.13	0.97^{***}	−0.06
20-Per-30	13.46	21	115	1.67	3.10	0.73	0.41	0.37	0.94^{***}	0.25
20-Per-21	13.41	17	118	1.88	1.59	0.57	0.70	0.38	0.73^{***}	−0.05
20-Per-40	13.36	17	118	1.56	6.05	0.39	0.80	−0.06	0.97^{***}	−0.15
20-Nan-01	12.94	15	86	1.69	5.25	0.42	0.76	0.73^{**}	0.96^{***}	0.70^{**}
20-Per-05[+]	12.87	28	118			0.77	0.36	−0.21	0.96^{***}	−0.23
20-Per-12	12.70	13	84	1.68	5.32	0.37	0.56	0.61^{*}	0.82^{***}	0.41
20-Per-03	12.68	19	95	1.53	4.48	0.39	0.71	0.87^{***}	0.72^{***}	0.56^{*}
20-Per-35	12.60	11	86	1.10	5.27	0.28	0.35	0.40	0.93^{***}	0.34
20-Per-07	12.43	12	87	1.37	5.16	0.26	0.32	0.60^{*}	1.00^{***}	0.60^{*}
20-Per-10	12.32	14	87	2.32	4.35	0.33	0.37	0.64^{*}	0.96^{***}	0.62^{*}
20-Per-09	12.28	15	86	1.54	2.33	0.21	0.56	0.53^{*}	0.93^{***}	0.56^{*}
20-Per-36	12.20	19	92	1.79	6.28	0.40	0.90	0.75^{***}	0.90^{***}	0.61^{**}
20-Per-33	12.15	22	93	1.20	3.10	0.27	1.39	0.45^{*}	−0.25	−0.26
20-Per-08	11.84	15	87	1.56	1.84	0.30	0.74	0.77^{***}	0.95^{***}	0.69^{**}
20-Per-32[+]	11.82	12	89			0.26	0.91	0.19	0.66^{*}	−0.12
20-Per-01	11.75	15	81	0.46	4.66	0.40	0.85	0.07	0.98^{***}	0.02
20-Per-45	11.72	19	92	0.93	6.32	0.36	1.06	−0.17	0.98^{***}	−0.13
20-Per-06	11.56	19	91	0.76	5.29	0.52	1.55	0.41	0.92^{***}	0.28
20-Per-15[+]	11.54	18	85			0.22	0.84	0.54^{*}	0.15	0.04
20-Per-04	11.47	14	86	0.89	4.54	0.16	0.96	0.40	0.24	−0.03
20-Per-02	11.44	14	87	0.50	4.62	0.56	1.25	−0.23	0.91^{***}	−0.30
20-Per-37[+]	11.41	19	84			0.30	1.44	0.68^{**}	0.75^{***}	0.82^{***}
20-Per-29	11.29	16	84	1.03	4.88	0.52	1.11	−0.15	0.88^{***}	−0.09
20-Per-44	11.26	14	97	1.41	3.96	0.31	0.62	0.49	0.97^{***}	0.47
20-Per-13	11.22	16	80	0.50	4.47	0.94	0.78	-0.54^{*}	0.97^{***}	-0.57^{*}
20-Per-25[+]	11.19	15	87			0.87	0.75	-0.55^{*}	0.95^{***}	-0.60^{*}
20-Per-38	11.18	13	86	1.49	0.96	0.57	1.85	0.27	−0.04	-0.82^{***}
20-Per-48	11.13	14	90	0.30	7.26	0.59	0.73	−0.02	1.00^{***}	−0.02
20-Per-31	11.08	17	83	1.93	1.00	0.29	0.62	0.22	0.75^{***}	0.18
20-Per-14	11.07	15	85	0.31	2.87	0.49	1.15	−0.04	0.73^{**}	−0.40
20-Per-11	11.00	23	86	1.14	3.71	0.28	0.61	0.62^{**}	0.98^{***}	0.60^{**}
20-Per-20	10.90	13	81	0.94	4.08	0.50	0.58	−0.47	0.99^{***}	−0.52
20-Per-16	10.77	16	86	1.20	3.33	0.47	0.69	−0.17	0.97^{***}	−0.21
20-Per-34	10.63	19	84	0.35	3.93	0.20	0.63	0.34	0.87^{***}	0.15
20-Per-39	10.60	12	84	0.57	2.23	0.35	0.77	0.52	0.85^{***}	0.42
20-Per-42	10.41	18	82	0.11	4.50	0.47	0.68	-0.66^{**}	0.96^{***}	-0.66^{**}
20-Per-41	9.86	13	83	−0.58	6.31	0.67	0.97	-0.78^{**}	0.99^{***}	-0.77^{**}
YFT Combined	***12.69***	***18***	***100***	***1.27***	***4.47***	***0.42***	***0.82***	$\boldsymbol{0.34^{***}}$	$\boldsymbol{0.75^{***}}$	$\boldsymbol{0.12^{***}}$

[+] core lost during analysis

$^{*}p \leq 0.05$, $^{**}p \leq 0.01$, $^{***}p \leq 0.001$

Table 3: Individual BLFT information ordered by decreasing eye lens diameter (ELD). Number of eye lens laminae (ELL), fork length (FL), lifetime isotopic change (LC), mean absolute deviation from predicted isotopic values (MAD), and Spearman rank correlation coefficients (ρ) are listed. Means were calculated for ELD, ELL, FL, and LC, and MAD and correlation coefficients were calculated for all BLFT combined.

Fish ID	ELD (mm)	ELL	FL (cm)	LC $\delta^{13}C$	LC $\delta^{15}N$	MAD $\delta^{13}C$	MAD $\delta^{15}N$	$\delta^{13}C$ vs LM ρ	$\delta^{15}N$ vs LM ρ	$\delta^{15}N$ vs $\delta^{13}C$ ρ
22-SL9-150-25	16.80	21	88	1.15	10.61	0.49	1.39	0.26	0.98^{***}	0.26
20-Nan-03	13.97	22	71	0.94	7.73	0.29	0.69	0.31	0.99^{***}	0.29
20-Nan-07^{+}	13.95	18	66			0.33	0.91	−0.43	0.98^{***}	-0.54^{*}
22-T-01	13.21	16	76	0.70	3.09	0.21	1.30	0.07	0.66^{**}	0.15
20-Per-24	13.05	20		0.48	4.34	0.45	0.88	−0.35	0.95^{***}	-0.46^{*}
20-Nan-04	12.92	15		1.81	6.32	0.53	0.83	0.11	0.96^{***}	0.01
20-Nan-05	12.30	16	59	0.45	5.15	0.28	0.76	−0.09	0.95^{***}	−0.07
20-Nan-15	12.16	17	60	0.59	4.26	0.41	0.78	−0.41	0.88^{***}	−0.34
20-Nan-17	11.91	21	62	0.25	4.59	0.32	0.46	−0.07	0.99^{***}	−0.09
20-Nan-08	11.67	19	62	0.52	4.17	0.28	0.50	0.19	0.79^{***}	−0.18
20-Per-43	11.50	15	58	0.18	4.91	0.16	0.81	0.08	0.98^{***}	0.03
20-Nan-18	11.38	13	59	0.31	4.71	0.31	0.80	0.42	0.96^{***}	0.34
20-Nan-19	11.19	16	58	0.59	5.25	0.24	0.63	−0.02	0.99^{***}	−0.06
20-Nan-12	11.08	21	59	0.41	6.41	0.41	0.92	-0.63^{**}	0.95^{***}	-0.60^{**}
20-Nan-09	11.03	13	58	0.62	4.48	0.22	0.82	−0.04	0.95^{***}	−0.16
20-Nan-10^{+}	11.00	15	59			0.32	0.40	0.81^{***}	1.00^{***}	0.80^{***}
20-Nan-11	10.93	16	57	0.30	4.44	0.30	0.88	0.18	0.97^{***}	0.13
20-Per-27	10.91	20	61	0.85	3.03	0.38	0.60	0.56^{**}	0.88^{***}	0.28
20-Nan-20	10.89	14	59	0.52	5.04	0.22	0.77	0.45	1.00^{***}	0.45
20-Nan-16	10.73	16	62	1.61	3.84	0.38	0.83	0.13	0.94^{***}	0.03
20-Per-23	10.65	15		0.12	5.27	0.33	0.84	-0.70^{**}	0.98^{***}	-0.80^{***}
20-Nan-14	10.47	22	58	0.88	5.38	0.53	0.81	−0.35	0.98^{***}	−0.42
20-Nan-13	10.28	14	59	−0.13	4.90	0.18	0.74	−0.09	1.00^{***}	−0.10
20-Nan-21	10.12	10	56	0.64	4.41	0.41	1.56	−0.16	0.90^{***}	−0.43
20-Nan-23^{+}	10.00	9	57			0.54	1.92	0.78^{*}	0.92^{***}	0.63
20-Hoov-01	9.99	13	57	0.50	3.74	0.58	1.19	−0.42	0.88^{***}	−0.40
20-Per-28	9.86	18		0.53	6.00	0.53	0.75	−0.45	0.97^{***}	−0.40
20-Hoov-02	9.03	12	56	−1.61	6.25	0.64	0.59	-0.75^{**}	0.99^{***}	-0.78^{**}
20-Nan-24	8.75	16	53	0.52	4.64	0.27	1.39	0.78^{***}	1.00^{***}	0.78^{***}
20-Nan-06^{+}	8.43	8	48			0.61	0.52	0.62	1.00^{***}	0.62
20-Per-26	8.38	14	56	0.25	3.57	0.20	0.62	−0.06	0.89^{***}	−0.31
BLFT Combined	***11.24***	***16***	***62***	***0.55***	***4.98***	***0.36***	***0.85***	***0.02***	***0.88****	***−0.15****

$^{+}$ core lost during analysis

$^{*}p \leq 0.05$, $^{**}p \leq 0.01$, $^{***}p \leq 0.001$

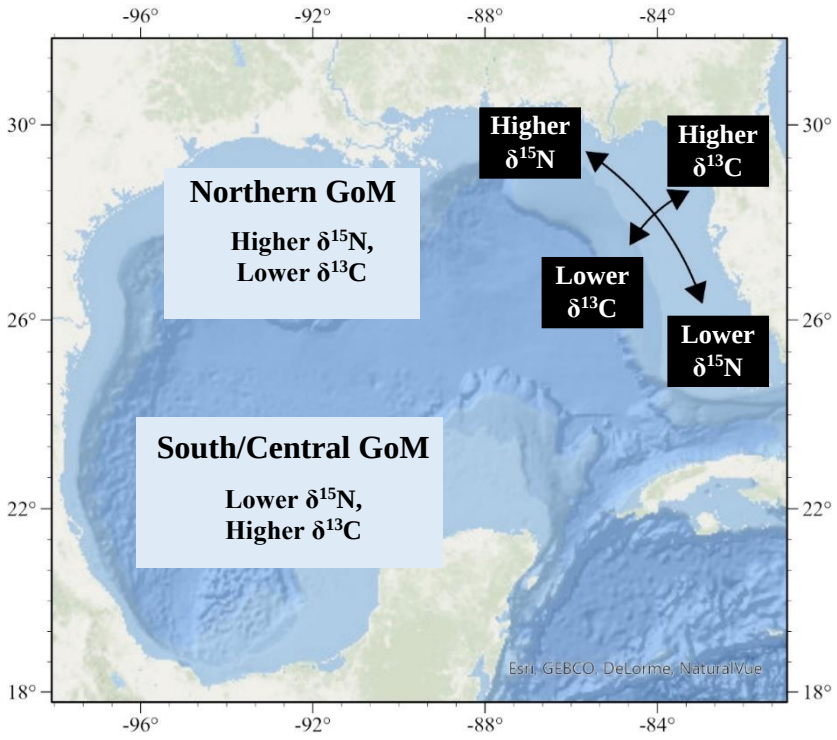

Figure 1: General $\delta^{13}C$ and $\delta^{15}N$ trends in the Gulf of Mexico. Broad trends from the Northern and South/Central Gulf of Mexico (GoM) derived from Alvarado et al (2020) zooplankton-based data and West Florida Shelf trends depicted by the arrows from Radabaugh and Peebles (2013) fish muscle-based data.

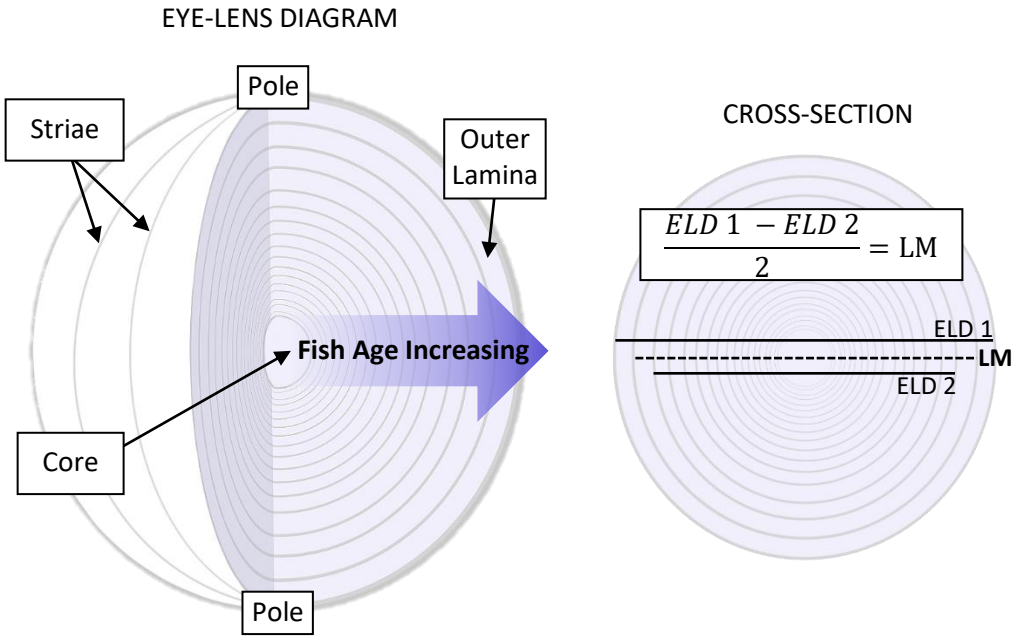

Figure 2: Basic fish eye-lens diagram and cross-section describing common terms, eye-lens diameter (ELD), and laminar midpoint (LM).

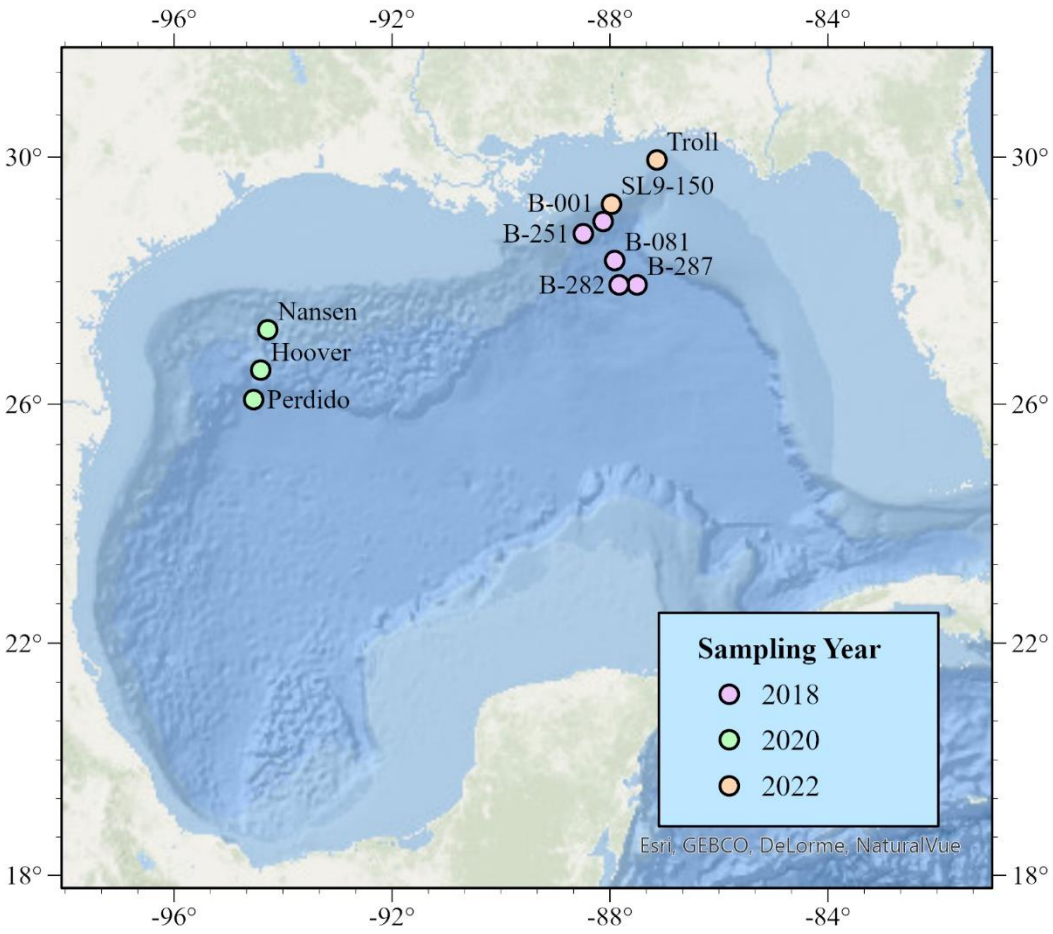

Figure 3: Map of Gulf of Mexico depicting the stations and locations where tuna were caught.

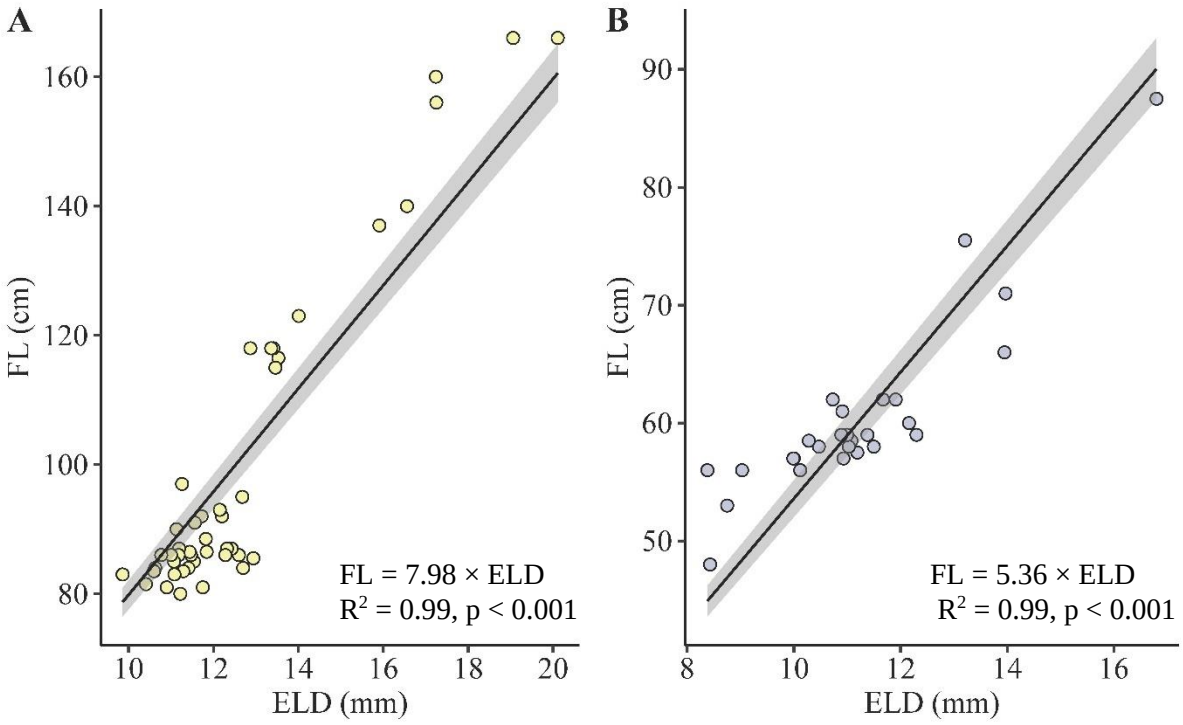

Figure 4: Linear regression forced through the origin relating eye lens diameter (ELD) at time of capture and fork length (FL) at time of capture for YFT (A) and BLFT (B).

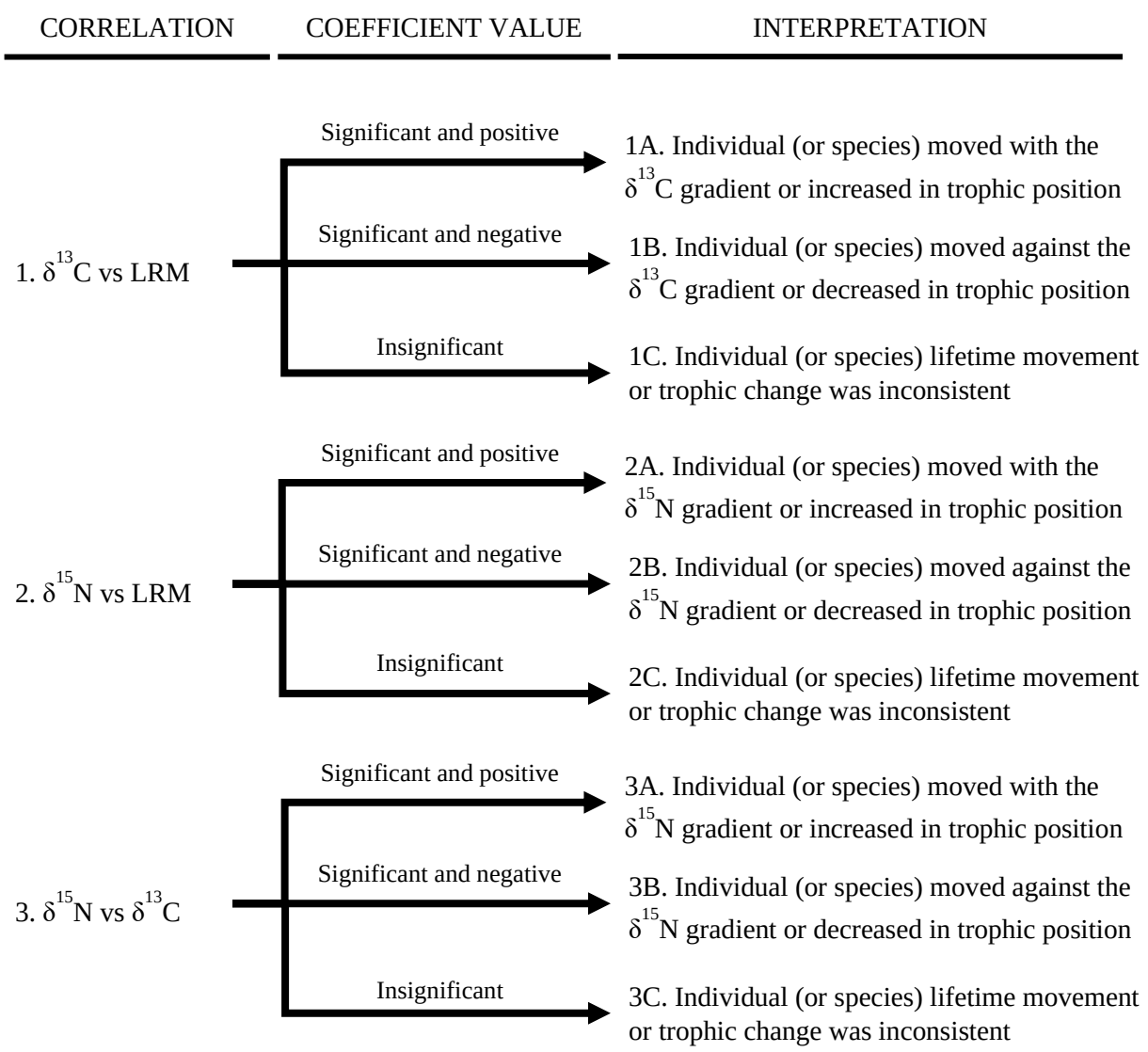

Figure 5: Interpretations of movement across isotopic gradients and trophic changes based on significance of correlations between variables. Adapted from Vecchio et al. 2021.

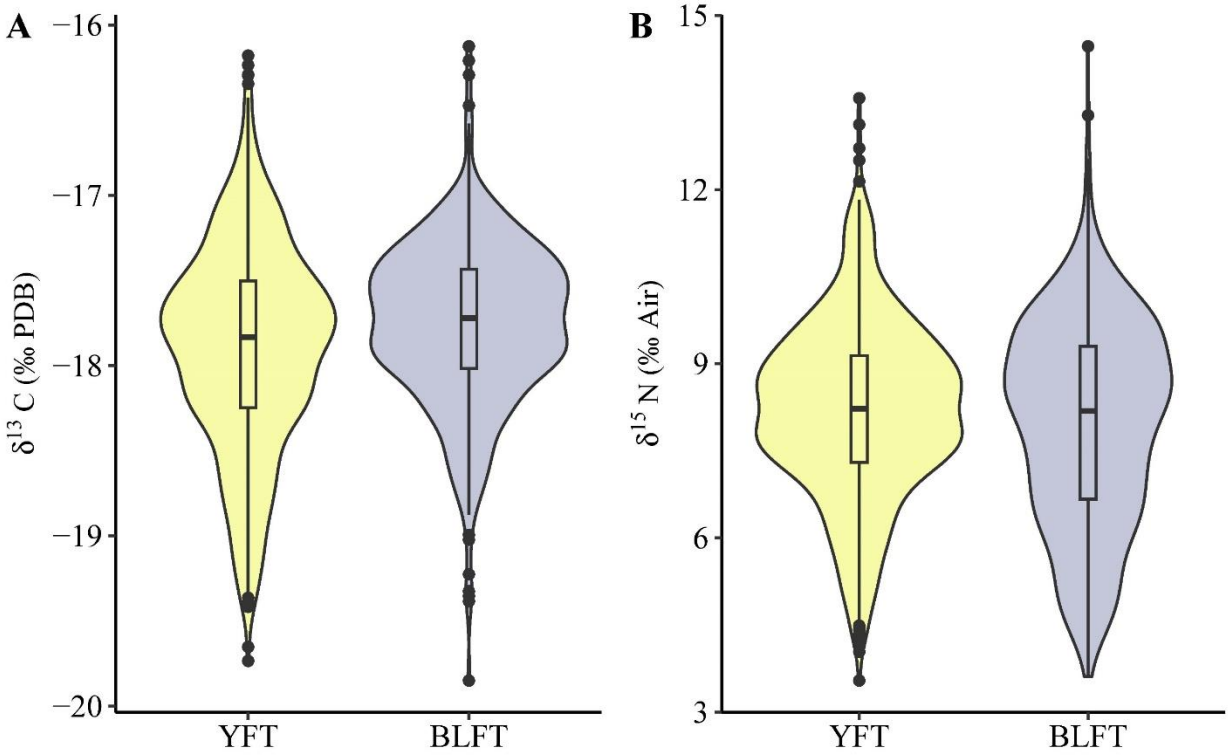

Figure 6: Distribution and range of carbon (A) and nitrogen (B) isotopic values for all YFT and BLFT laminae. Mean is shown within the embedded boxplot.

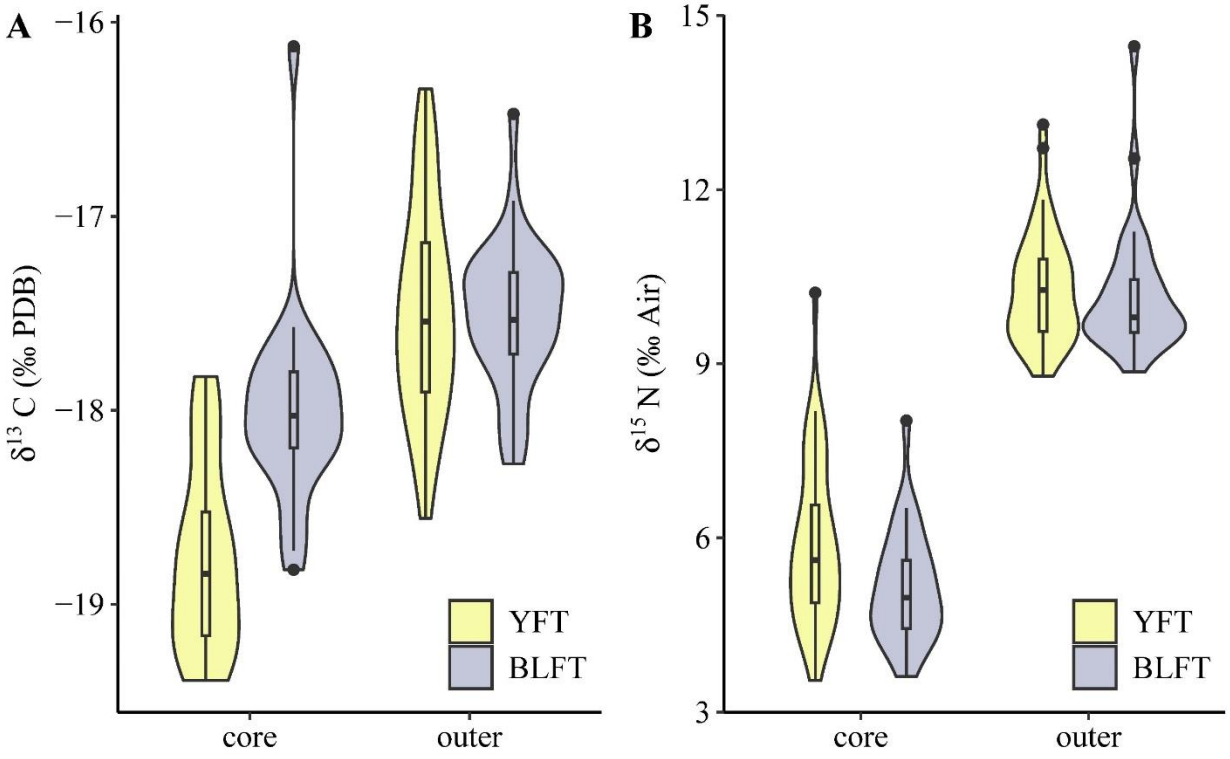

Figure 7: Distribution and range of carbon (A) and nitrogen (B) isotopic values for YFT and BLFT core and outer laminae. Six YFT cores and four BLFT cores were lost during analysis and are not included on this graph. Mean is shown within the embedded boxplot.

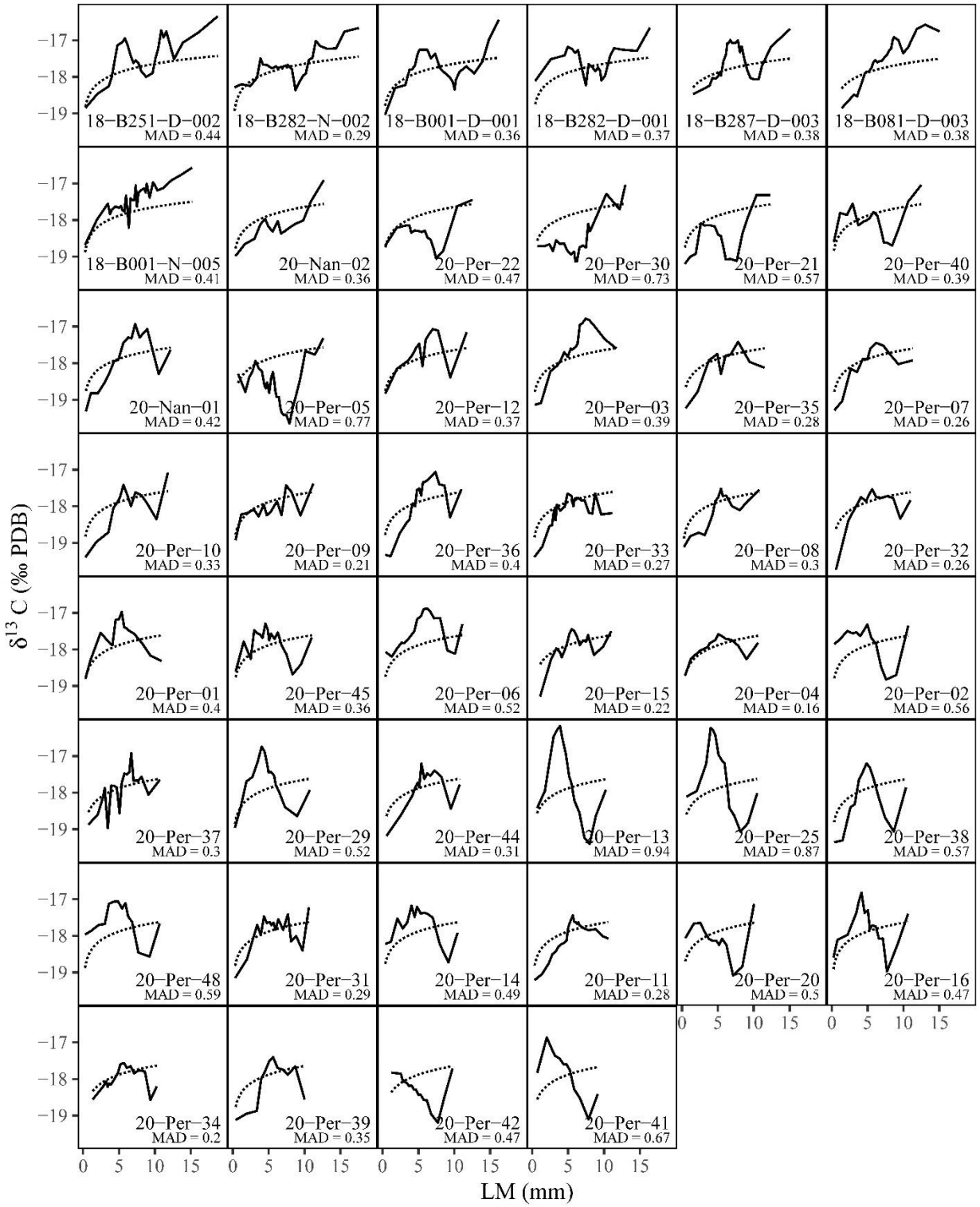

Figure 8: Individual YFT lifetime carbon isotopic profiles (solid line) compared to the predicted logarithmic relationship determined from all YFT laminae combined (dotted line). Profiles are arranged by eye lens diameter (ELD). Laminar midpoint (LM) is used as a proxy for age. Mean absolute deviation of observed values from predicted values is listed for each individual.

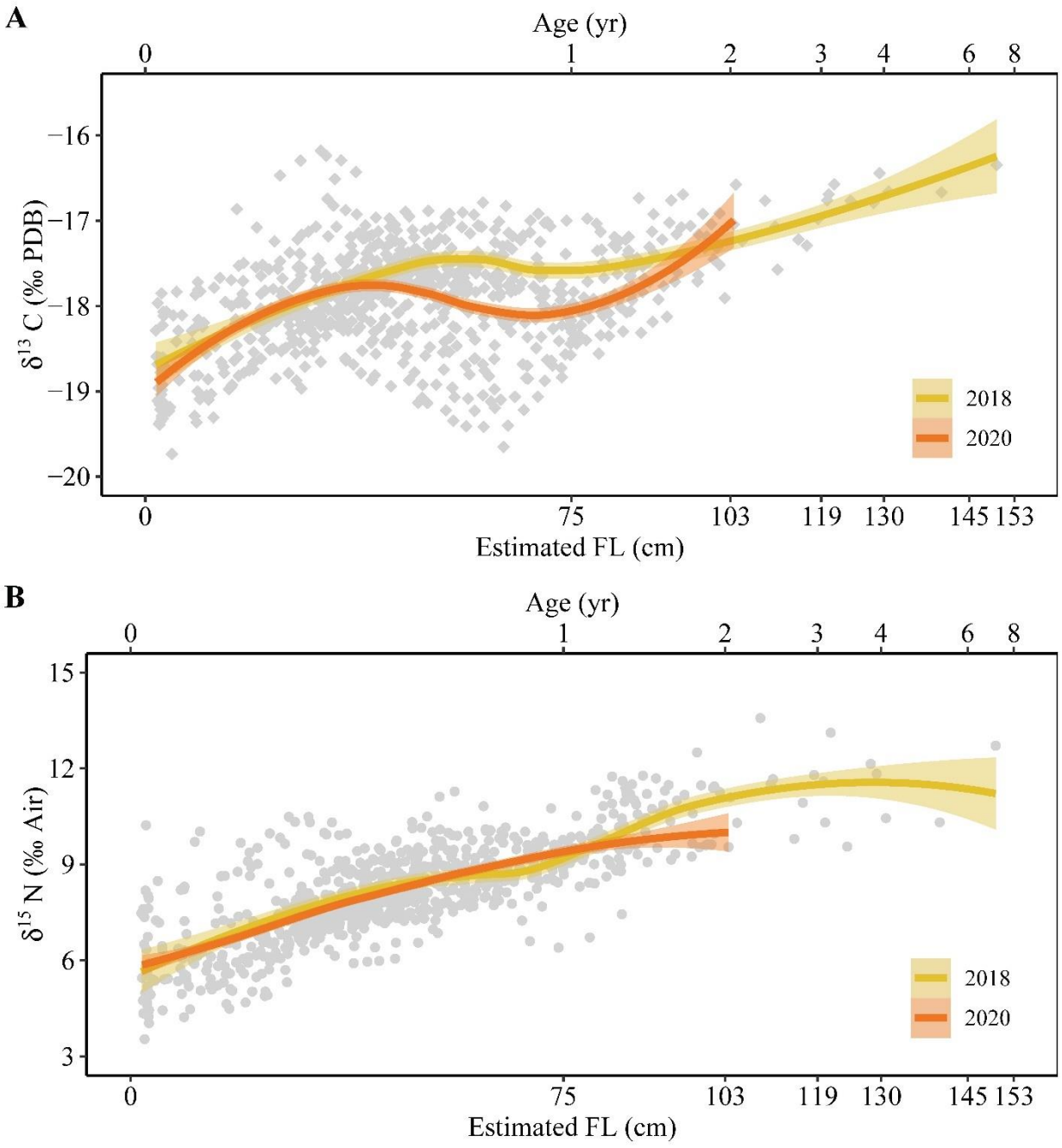

Figure 9: LOESS curves for YFT carbon isotope values (A) and nitrogen isotopic values (B), separated by year.

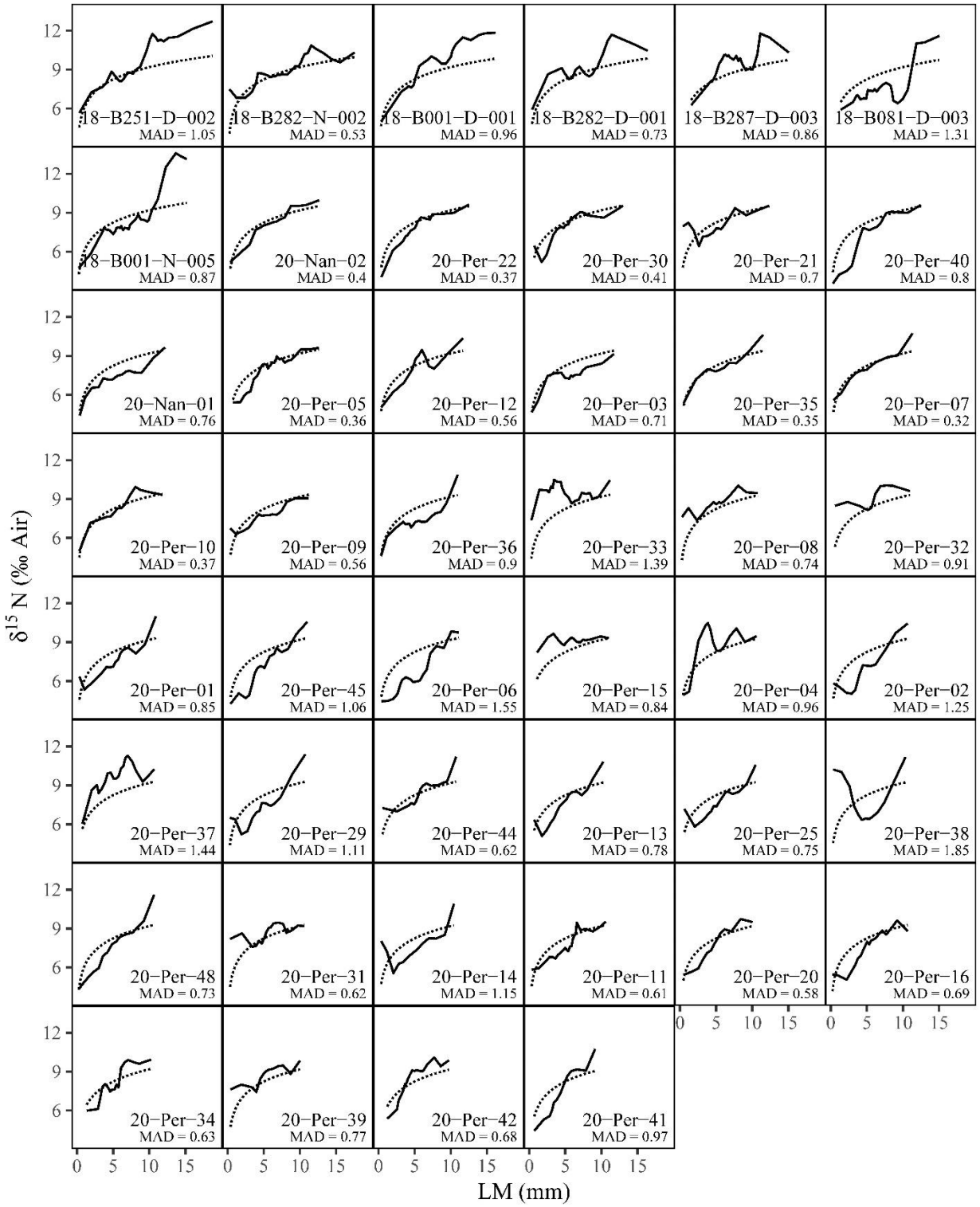

Figure 10: Individual YFT lifetime nitrogen isotopic profiles (solid line) compared to the predicted logarithmic relationship determined from all YFT laminae combined (dotted line). Profiles are arranged by eye lens diameter (ELD). Laminar midpoint (LM) is used as a proxy for age. Mean absolute deviation of observed values from predicted values is listed for each individual.

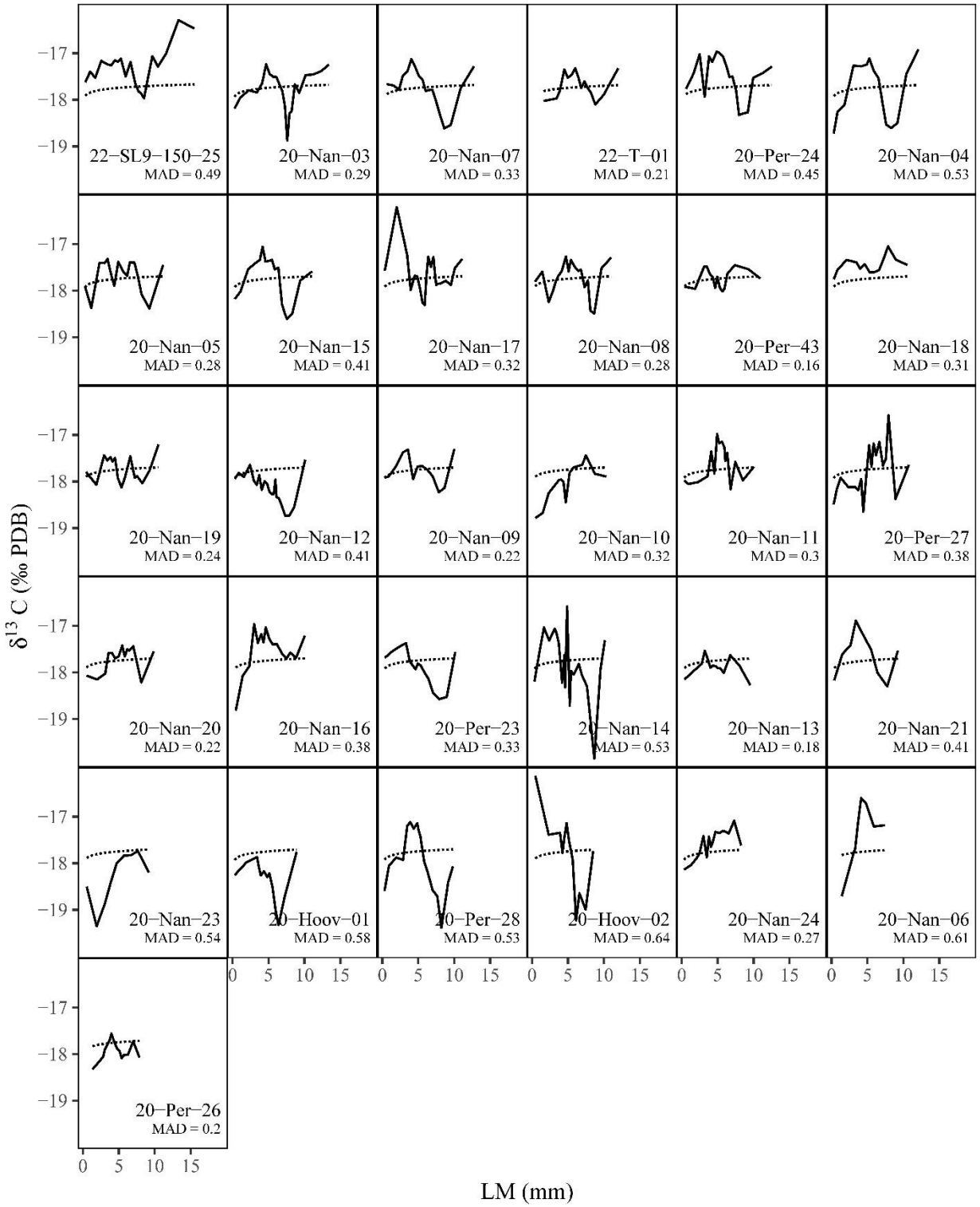

Figure 11: Individual BLFT lifetime carbon isotopic profiles (solid line) compared to the predicted logarithmic relationship determined from all BLFT laminae combined (dotted line). Profiles are arranged by eye lens diameter (ELD). Laminar midpoint (LM) is used as a proxy for age. Mean absolute deviation of observed values from predicted values is listed for each individual.

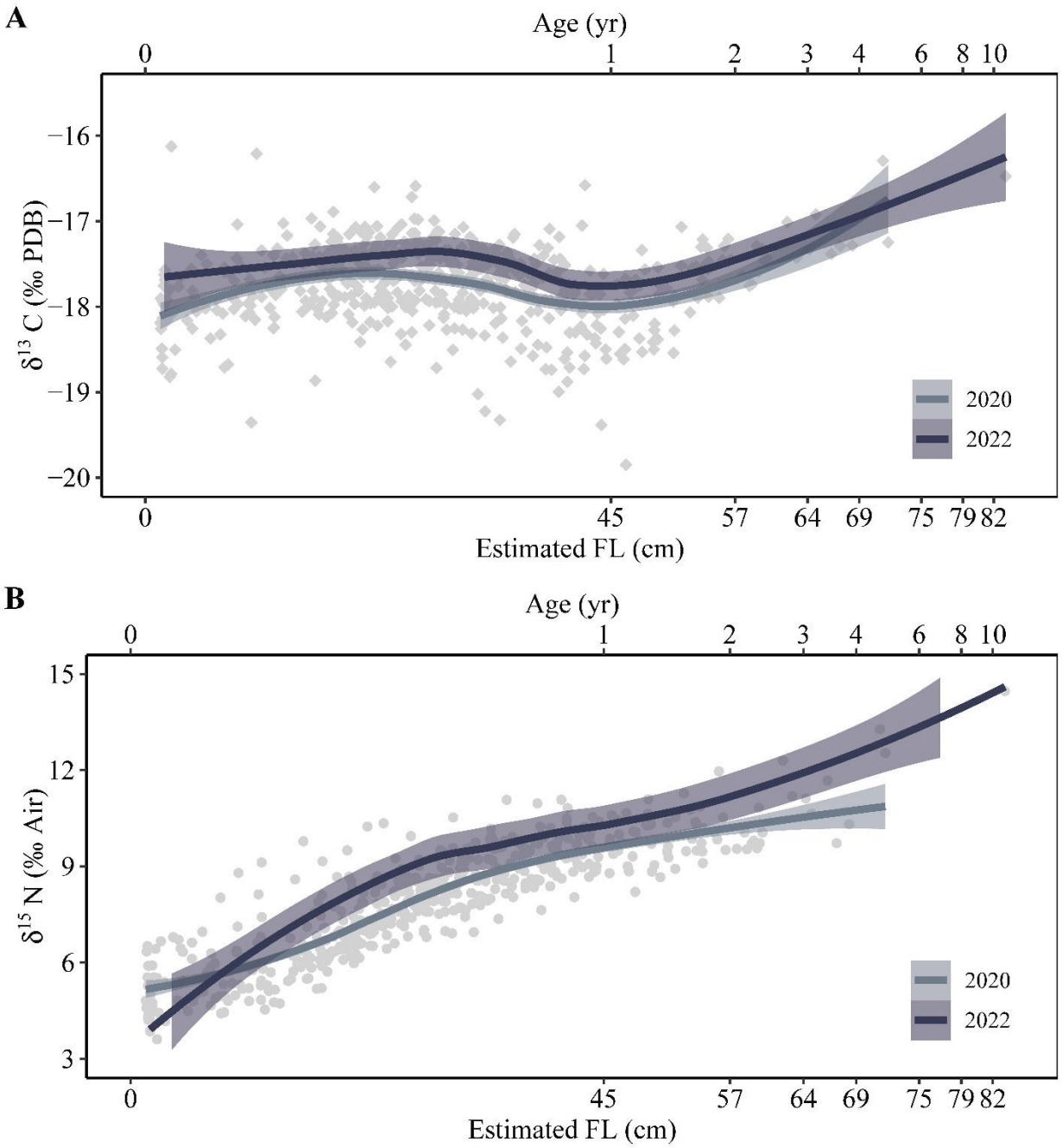

Figure 12: LOESS curves for BLFT carbon isotope values (A) and nitrogen isotopic values (B), separated by year.

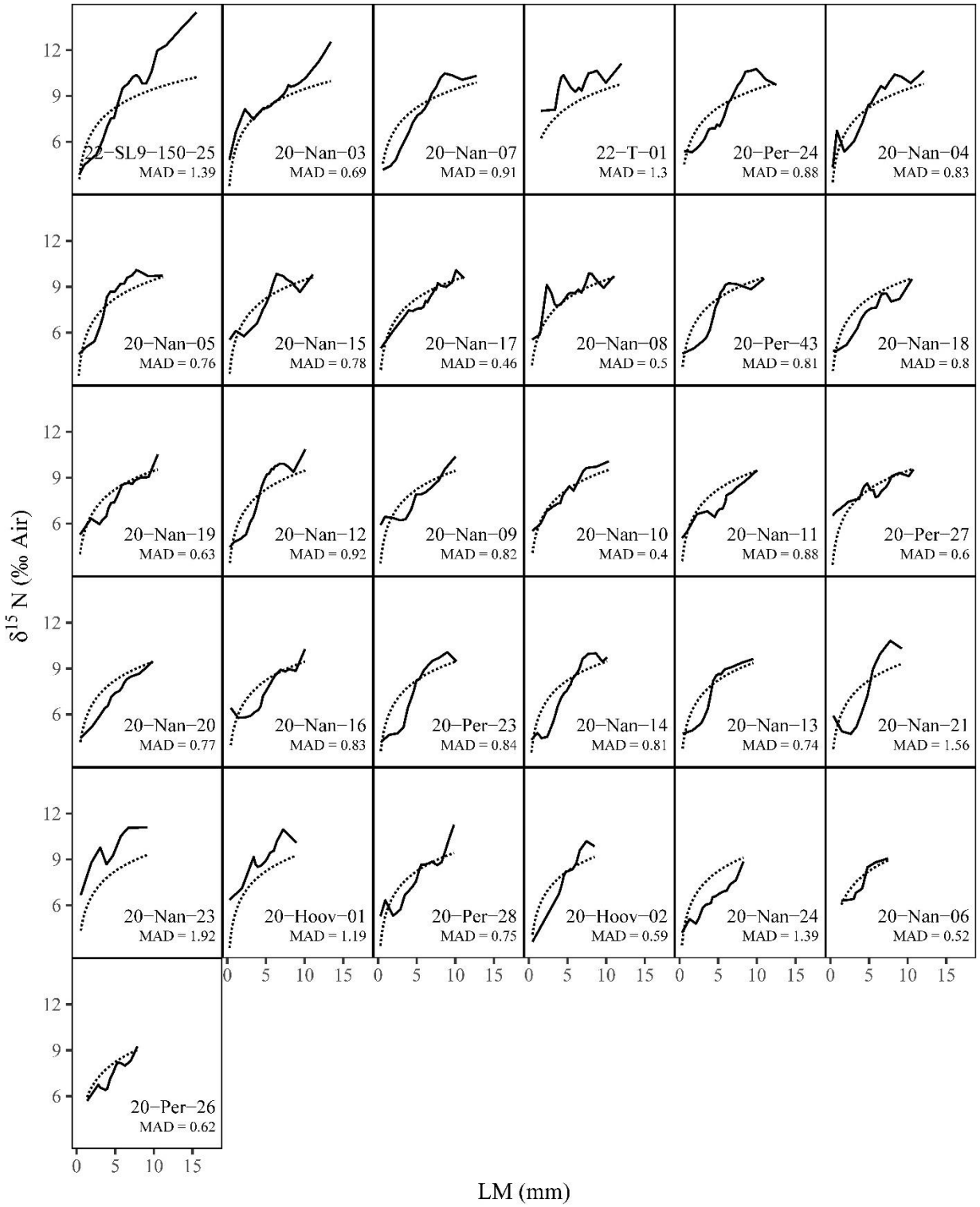

Figure 13: Individual BLFT lifetime nitrogen isotopic profiles (solid line) compared to the predicted logarithmic relationship determined from all BLFT laminae combined (dotted line). Profiles are arranged by eye lens diameter (ELD).). Laminar midpoint (LM) is used as a proxy for age. Mean absolute deviation of observed values from predicted values is listed for each individual.

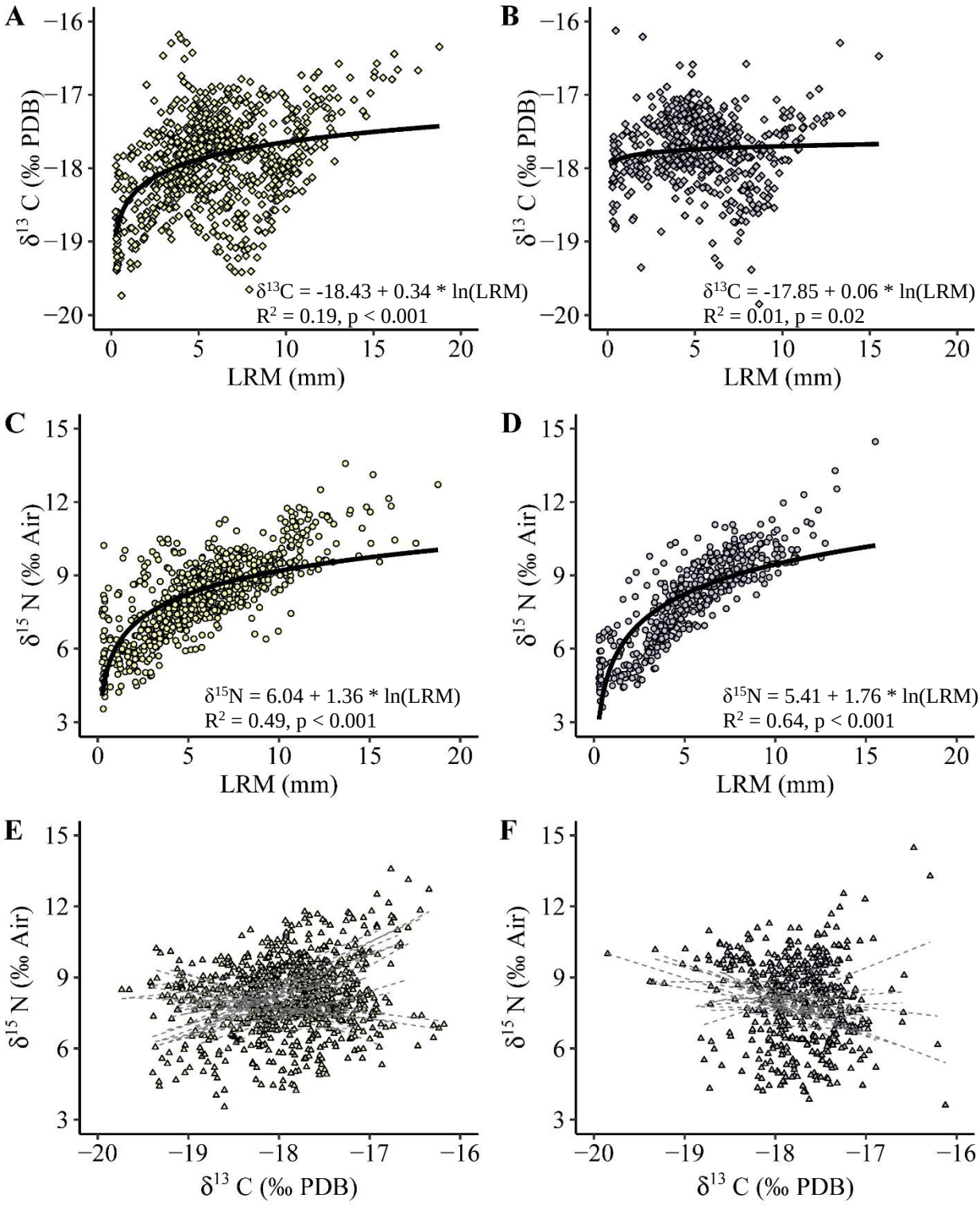

Figure 14: Profiles containing all laminae for each species: $\delta^{13}C$ values vs laminar midpoint (LM) for YFT (**A**) and BLFT (**B**), $\delta^{15}N$ values vs LM for YFT (**C**) and BLFT (**D**), and $\delta^{15}N$ vs $\delta^{13}C$ values for YFT (**E**) and BLFT (**F**). Solid lines in lifetime profiles indicate the predicted logarithmic relationship. Dashed lines in isotopic profiles indicate the slope of the mixed linear effect model for each individual.

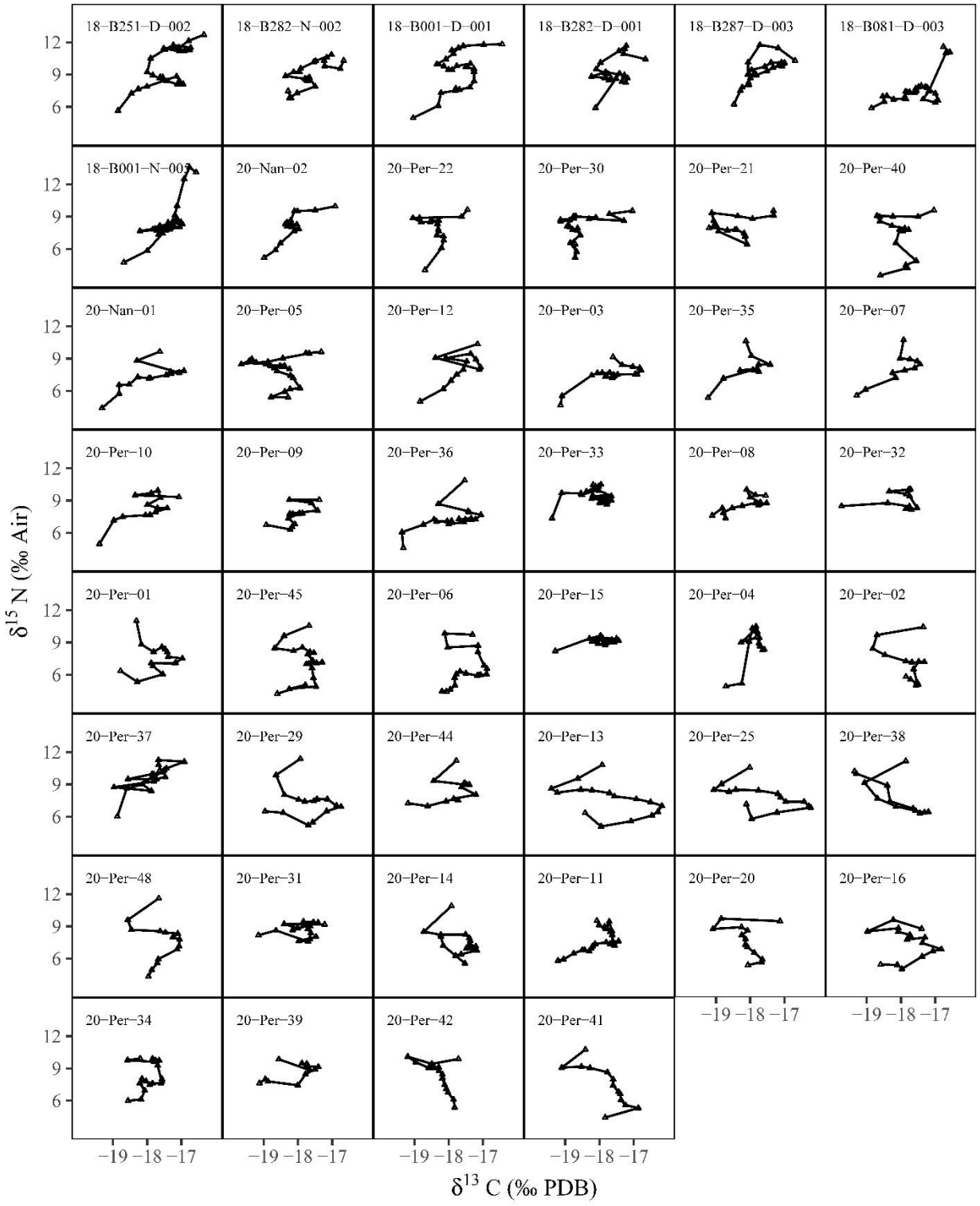

Figure 15: Individual YFT lifetime nitrogen and carbon isotopic profiles over time. Profiles are arranged by eye lens diameter (ELD).

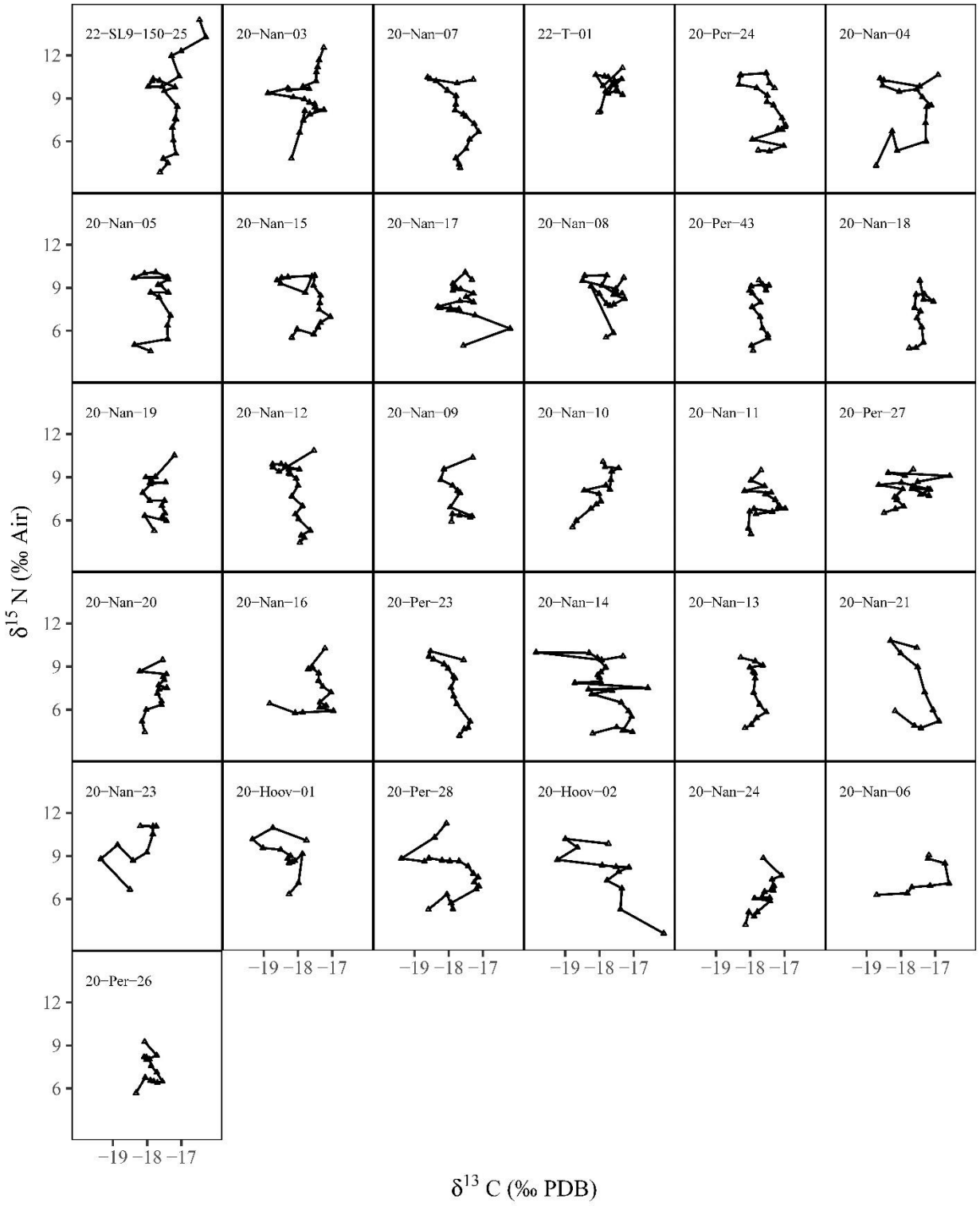

Figure 16: Individual BLFT lifetime nitrogen and carbon isotopic profiles over time. Profiles are arranged by eye lens diameter (ELD).

REFERENCES

Albuquerque F, Navia A, Vaske Jr T, Crespo Neto O, Hazin F (2019) Trophic ecology of large pelagic fish in the Saint Peter and Saint Paul Archipelago, Brazil. Marine and Freshwater Research 70:1402–1418

Arocha F, Lee D, Marcano L, Marcano J (2001) Update information on the spawning of yellowfin tuna, *Thunnus albacares*, in the western central Atlantic. Collective Volume of Scientific Papers ICCAT 52: 167–176

Bates D, Mächler M, Bolker BM, Walker SC (2015) Fitting linear mixed-ffects models using lme4. Journal of Statistical Software 67:1-48

Boyce DG, Tittensor DP, Worm B (2008) Effects of temperature on global patterns of tuna and billfish richness. Marine Ecology Progress Series 355:267–276

Chen Y (2017) Fish resources of the Gulf of Mexico. In: Ward CH (ed) Habitats and biota of the Gulf of Mexico: before the Deepwater Horizon oil spill: Volume 2: fish resources, fisheries, sea turtles, avian resources, marine mammals, diseases and mortalities. Springer New York, New York, NY

Collette BB, Nauen CE (1983) FAO species catalogue: Vol. 2 scombrids of the world. An annotated and illustrated catalogue of tunas, mackarels, bonitos and related species known to date. FAO Fish Synop 125(2):85–86

Cornic M, Rooker JR (2018) Influence of oceanographic conditions on the distribution and abundance of blackfin tuna (T*hunnus atlanticus*) larvae in the Gulf of Mexico. Fisheries Research 201:1–10

Cornic M, Rooker JR (2021) Temporal shifts in the abundance and preferred habitats of yellowfin and bigeye tuna larvae in the Gulf of Mexico. Journal of Marine Systems 217:103524

Cornic M, Smith BL, Kitchens LL, Alvarado Bremer JR, Rooker JR (2017) Abundance and habitat associations of tuna larvae in the surface water of the Gulf of Mexico. Hydrobiologia 806:29–46

Curtis JS, Albins MA, Peebles EB, Stallings CD (2020) Stable isotope analysis of eye lenses from invasive lionfish yields record of resource use. Marine Ecology Progress Series 637:181–194

Edwards R, Sulak K (2006) New paradigms for yellowfin tuna movements and distributions – implications for the Gulf and Caribbean region. Proceedings of the Gulf and Caribbean Fisheries Institute 57:283–296

Espinosa-Fuentes M, Flores-Coto C, Zavala-García F, Sanvicente-Añorve L, Funes-Rodríguez R (2013) Seasonal vertical distribution of fish larvae in the southern Gulf of Mexico. Hidrobiológica 23:42–59

Fenton J, Ellis JM, Falterman B, Kerstetter DW (2015) Habitat utilization of blackfin tuna, *Thunnus atlanticus*, in the north-central Gulf of Mexico. Environmental Biology of Fishes 98:1141–1150

Fry B (2006) Stable isotope ecology. Springer Science+Business Media, LLC, 233 Spring Street, New York, NY 10013, USA

Graham BS, Grubbs D, Holland K, Popp BN (2007) A rapid ontogenetic shift in the diet of juvenile yellowfin tuna from Hawaii. Marine Biology 150:647–658

Graham BS, Koch PL, Newsome SD, McMahon KW, Aurioles D (2010) Using isoscapes to trace the movements and foraging behavior of top predators in oceanic ecosystems. In: West JB, Bowen GB, Dawson TE, Tu KP (eds) Isoscapes: understanding movement, pattern and process on Earth through isotope mapping. Springer Science+Business Media, LLC, 233 Spring Street, New York, NY 10013, USA, p 299–318

Greiling TMS, Clark JI (2012) New insights into the mechanism of lens development using zebra fish. International Review of Cell and Molecular Biology 296:1–61

Grimes C, Finucane J (1991) Spatial distribution and abundance of larval and juvenile fish, chlorophyll and macrozooplankton around the Mississippi River discharge plume, and the role of the plume in fish recruitment. Marine Ecology Progress Series 75:109–119.

Gutierrez, EM (2022) Age and growth of blackfin tuna (*Thunnus atlanticus*) in the Gulf of Mexico. [Unpublished Master's thesis]. LSU Master's Theses. 5536.

Hansson S, Hobbie JE, Elmgren R, Larsson U, Fry B, Johansson S (1997) The stable nitrogen isotope ratio as a marker of food-web interactions and fish migration. Ecology 78:2249–2257

Harada Y, Ito S, Ogawa NO, Yoshikawa C, Ishikawa NF, Yoneda M, Ohkouchi N (2022) Compound-specific nitrogen isotope analysis of amino acids in eye lenses as a new tool to reconstruct the geographic and trophic histories of fish. Frontiers in Marine Science 8:796532

Headley BM, Oxenford HA, Peterson MS, Fanning P (2009) Size related variability in the summer diet of the blackfin tuna (*Thunnus atlanticus* Lesson, 1831) from Tobago, the Lesser Antilles. Journal of Applied Ichthyology 25:669–675

Hobson KA, Barnett-Johnson R, Cerling T (2010) Using isoscapes to track animal migration. In: West JB, Bowen GJ, Dawson TE, Tu KP (eds) Isoscapes: understanding movement, pattern, and process on Earth through isotope mapping. Springer Netherlands, Dordrecht

Hoolihan JP, Wells RJD, Luo J, Falterman B, Prince ED, Rooker JR (2014) Vertical and horizontal movements of yellowfin tuna in the gulf of mexico. Marine and Coastal Fisheries: Dynamics, Management, and Ecosystem Science 6:211–222

ICCAT (2019) Report of the 2019 ICCAT Yellowfin Tuna Stock Assessment Meeting. International Commission for the Conservation of Atlantic Tunas, Grand-Bassam, Cote d'Ivoire, July 8 to 16, 2019 (available at https://www.iccat.int/Documents/Meetings/Docs/2019/REPORTS/2019_YFT_SA_ENG.pdf)

Karnauskas M, Kelble CR, Regan S, Quenée C, Allee R, Jepson M, Freitag A, Craig JK, Carollo C, Barbero L, Trifonova N, Hanisko D, Zapfe G (2017) 2017 Ecosystem status report update for the Gulf of Mexico. NOAA Technical Memorandum NMFS-SEFSC-706, 51 p

Klimley AP, Jorgensen SJ, Muhlia-Melo A, Beavers SC (2003) The occurrence of yellowfin tuna (*Thunnus albacares*) at Espiritu Santo Seamount in the Gulf of California. Fishery Bulletin 101:684–692

Kurth BN, Peebles EB, Stallings CD (2019) Atlantic Tarpon (*Megalops atlanticus*) exhibit upper estuarine habitat dependence followed by foraging system fidelity after ontogenetic habitat shifts. Estuarine, Coastal and Shelf Science 225:106248

Lang KL, Grimes CB, Shaw RF (1994) Variations in the age and growth of yellowfin tuna larvae,*Thunnus albacares*, collected about the Mississippi River plume. Environmental Biology of Fishes 39:259–270

Le-Alvarado M, Romo-Curiel AE, Sosa-Nishizaki O, Hernández-Sánchez O, Barbero L, Herzka SZ (2021) Yellowfin tuna (*Thunnus albacares*) foraging habitat and trophic position in the Gulf of Mexico based on intrinsic isotope tracers. PLOS ONE 16:e0246082

Logan J, Haas H, Deegan L, Gaines E (2006) Turnover rates of nitrogen stable isotopes in the salt marsh mummichog, *Fundulus heteroclitus*, following a laboratory diet switch. Oecologia 147:391–395

Lovell, MS (2021) Seasonal variation in the feeding ecology of yellowfin tuna (*Thunnus albacares*) from the northern Gulf of Mexico [Unpublished Master's thesis]. LSU Master's Theses. 5398.

Madigan DJ, Litvin SY, Popp BN, Carlisle AB, Farwell CJ, Block BA (2012) Tissue turnover rates and isotopic trophic discrimination factors in the endothermic teleost, Pacific bluefin tuna (Thunnus orientalis). PLOS ONE 7:e49220

Matley JK, Fisk AT, Tobin AJ, Heupel MR, Simpfendorfer CA (2015) Diet-tissue discrimination factors and turnover of carbon and nitrogen stable isotopes in tissues of an adult predatory coral reef fish, *Plectropomus leopardus*. Rapid Communications in Mass Spectrometry 30:29–44

McCutchan JH, Lewis WM, Kendall C, McGrath CC (2003) Variation in trophic shift for stable isotope ratios of carbon, nitrogen, and sulfur. Oikos 102:378–390

Meath B, Peebles EB, Seibel BA, Judkins H (2019) Stable isotopes in the eye lenses of *Doryteuthis plei* (Blainville 1823): Exploring natal origins and migratory patterns in the eastern Gulf of Mexico. Continental Shelf Research 174:76–84

Montoya JP, Carpenter EJ, Capone DG (2002) Nitrogen fixation and nitrogen isotope abundances in zooplankton of the oligotrophic North Atlantic. Limnology and Oceanography 47:1617–1628

Murawski S, Hollander D, Gilbert S, Gracia A (2020) Deepwater oil and gas production in the Gulf of Mexico and related global trends. In: Murawski SA, Ainsworth CH, Gilbert S, Hollander DJ, Paris CB, Schlüter M, Wetzel DL (eds) Scenarios and responses to future deep oil spills. Springer Nature Switzerland AG, Gewerbestrasse 11, 6330 Cham, Switzerland p 16–32

NMFS (2022) Fisheries of the United States, 2020. U.S. Department of Commerce, NOAA Current Fishery Statistics No. 2020 (available at: https://www.fisheries.noaa.gov/national/sustainable-fisheries/fisheries-united-states)

NOAA Fisheries Office of Science and Technology (2020), Commercial Landings Query, Available at: www.fisheries.noaa.gov/foss, Accessed 01/23/2023

Oksanen J, Simpson G, Blanchet F, Kindt R, Legendre P, Minchin P, O'Hara R, Solymos P, Stevens M, Szoecs E, Wagner H, Barbour M, Bedward M, Bolker B, Borcard D, Carvalho G, Chirico M, De Caceres M, Durand S, Evangelista H, FitzJohn R, Friendly M, Furneaux B, Hannigan G, Hill M, Lahti L, McGlinn D, Ouellette M, Ribeiro Cunha E, Smith T, Stier A, Ter Braak C, Weedon J (2022) _vegan: Community Ecology Package_. R package version 2.6-4

Olson R, Watters G (2003) A model of the pelagic ecosystem in the eastern tropical Pacific Ocean. Inter-American Tropical Tuna Commission, Bulletin 22:133–218

Orbesen ES, Snodgrass D, Shideler GS, Brown CA, Walter JF (2017) Diurnal patterns in Gulf of Mexico epipelagic predator interactions with pelagic longline gear: Implications for target species catch rates and bycatch mitigation. Bulletin of Marine Science 93:573–589

Ortiz M (2017) Review and analyses of tag releases and recaptures of yellowfin tuna ICCAT DB. Collective Volumes of Scientific Papers, ICCAT 73:228–243

Pacicco AE, Allman RJ, Lang ET, Murie DJ, Falterman BJ, Ahrens R, Walter JF, III (2021) Age and growth of yellowfin tuna in the U.S. Gulf of Mexico and Western Atlantic. Marine and Coastal Fisheries: Dynamics, Management, and Ecosystem Science 13:345–336

Peebles E, Hollander D (2020) Combining isoscapes with tissue-specific isotope records to recreate the geographic histories of fish. In: Murawski SA, Ainsworth CH, Gilbert S, Hollander DJ, Paris CB, Schlüter M, Wetzel DL (eds) Scenarios and responses to future deep oil spills. Springer Nature Switzerland AG, Gewerbestrasse 11, 6330 Cham, Switzerland p 203–218

Popp BN, Graham BS, Olson RJ, Hannides CCS, Lott MJ, López-Ibarra GA, Galván-Magaña F, Fry B (2007) Insight into the trophic ecology of yellowfin tuna, *Thunnus albacares,* from compound-specific nitrogen isotope analysis of proteinaceous amino acids. In: Dawson TE, Siegwolf RT (eds) Terrestrial ecology, Book 1. Elsevier p 173–190

Post DM (2002) Using stable isotopes to estimate trophic position: models, methods, and assumptions. Ecology 83:703–718

Price ME, Randall MT, Sulak KJ, Edwards RE, Lamont MM (2022) Temporal and spatial relationships of yellowfin tuna to deepwater petroleum platforms in the Northern Gulf of Mexico. Marine and Coastal Fisheries: Dynamics, Management, and Ecosystem Science 14:e10213

Quaeck-Davies K, Bendall VA, MacKenzie KM, Hetherington S, Newton J, Trueman CN (2018) Teleost and elasmobranch eye lenses as a target for life-history stable isotope analyses. PeerJ 6:e4883

R Core Team (2022) R: A language and environment for statistical computing. R Foundation for Statistical Computing, Vienna, Austria

Radabaugh KR, Hollander DJ, Peebles EB (2013) Seasonal δ13C and δ15N isoscapes of fish populations along a continental shelf trophic gradient. Continental Shelf Research 68:112–122

Reglero P, Tittensor DP, Álvarez-Berastegui D, Aparicio-González A, Worm B (2014) Worldwide distributions of tuna larvae: revisiting hypotheses on environmental requirements for spawning habitats. Marine Ecology Progress Series 501:207–224

Richardson DE, Llopiz JK, Guigand CM, Cowen RK (2010) Larval assemblages of large and medium-sized pelagic species in the Straits of Florida. Progress in Oceanography 86:8–20

Ricker WE (1975) Computation and interpretation of biological statistics of fish populations. Bulletin of the Fisheries Research Board of Canada 191

Rudershausen PJ, Buckel JA, Edwards J, Gannon DP, Butler CM, Averett TW (2010) Feeding ecology of blue marlins, dolphinfish, yellowfin tuna, and wahoos from the north atlantic ocean and comparisons with other oceans. Transactions of the American Fisheries Society 139:1335–1359

Simpson SJ, Sims DW, Trueman CN (2019) Ontogenetic trends in resource partitioning and trophic geography of sympatric skates (Rajidae) inferred from stable isotope composition across eye lenses. Marine Ecology Progress Series 624:103–116

Snodgrass DJG, Orbesen ES, Walter JF, Hoolihan JP, Brown CA (2020) Potential impacts of oil production platforms and their function as fish aggregating devices on the biology of highly migratory fish species. Reviews in Fish Biology and Fisheries 30:405–422

Tzadik OE, Curtis JS, Granneman JE, Kurth BN, Pusack TJ, Wallace AA, Hollander DJ, Peebles EB, Stallings CD (2017) Chemical archives in fishes beyond otoliths: A review on the use of other body parts as chronological recorders of microchemical constituents for expanding interpretations of environmental, ecological, and life-history changes. Limnology and Oceanography: Methods 15:238–263

Vecchio JL, Peebles EB (2020) Spawning origins and ontogenetic movements for demersal fishes: An approach using eye-lens stable isotopes. Estuarine, Coastal and Shelf Science 246:107047

Vecchio JL, Ostroff JL, Peebles EB (2021) Isotopic characterization of lifetime movement by two demersal fishes from the northeastern Gulf of Mexico. Marine Ecology Progress Series 657:161–172

von Bertalanffy L (1938) A quantitative theory of organic growth (Inquiries on growth laws II). Human Biology 10:181- 213.

Wallace AA, Ellis GS, Peebles EB (2023) Reconstructions of individual fish trophic geographies using isotopic analysis of eye-lens amino acids. PLoS ONE 18(3): e0282669.

Wallace AA, Hollander DJ, Peebles EB (2014) Stable Isotopes in Fish Eye Lenses as Potential Recorders of Trophic and Geographic History. PLOS ONE 9:e108935

Weng KC, Stokesbury MJ, Boustany AM, Seitz AC, Teo SL, Miller SK, Block BA (2009) Habitat and behaviour of yellowfin tuna *Thunnus albacares* in the Gulf of Mexico determined using pop-up satellite archival tags. Journal of Fish Biology 74:1434–1449

Wistow GJ, Piatigorsky J (1988) Lens crystallins: the evolution and expression of proteins for a highly specialized tissue. Annual review of biochemistry 57:479–504

Wride MA (2011) Lens fibre cell differentiation and organelle loss: many paths lead to clarity. Philosophical transactions of the Royal Society of London Series B, Biological sciences 366:1219–1233